

RF-MEMS Actuated by the Lorentz Force

Jérôme LE NY

March 17, 2003

Contents

Introduction	5
I Preliminary Study	7
1 Actuation Techniques for RF MEMS	9
1.1 Electrostatic Actuation	9
1.2 Other Non Magnetic Actuation Techniques	10
1.3 A Magnetic Switch	10
2 Magnetic Materials for MEMS	13
2.1 Overview	13
2.2 Current State	14
2.2.1 Research Groups	14
2.2.2 Companies	15
3 Microsystems Actuated by Lorentz Forces	17
3.1 Introduction	17
3.2 Switches	17
3.3 Voltage Tunable Capacitor	18
3.4 Filters	18
3.5 Impossibility of Mixing	20
II Design of a Magnetically Actuated Switch	21
4 Design of the Magnetic Circuit	23
4.1 Introduction	23
4.2 Magnetic Circuit Design	23
4.2.1 Overview	23
4.2.2 Equations	24
4.3 Planar Configuration	26
4.3.1 Presentation of the Design	26
4.3.2 Impact of the Thickness on the Biasing of the Magnetic Circuit	29

4.4	Vertical Configuration and Packaging	30
4.4.1	Final Device	31
4.4.2	Process	31
4.4.3	Magnetic Characteristics of the Materials	31
4.4.4	Magnetic Simulation Results	33
5	Mechanical Analysis	35
5.1	Overview	35
5.2	Static Analysis	35
5.2.1	Bending of a Beam Subjected to a Uniform Load	35
5.2.2	Uniformly Loaded Beam in Contact with a Solid Wall	36
5.3	Dynamic Analysis	38
5.3.1	Electromagnetic Damping	38
5.3.2	Switching Speed. Transient Response of the Beam Subject to a Dual Magnetic and Electrostatic Actuation	40
5.3.3	Finite Elements Dynamics Simulation	44
III	Stability Study	45
6	Problems of Stability for a Beam in a Non Uniform Magnetic Field	47
6.1	Introduction	47
6.2	Potential Energy Associated with the Lorentz Forces	48
6.2.1	Work Done by the Lorentz Forces for a Portion of Lineic Circuit in \mathbf{B}_{ext}	48
6.2.2	Maxwell's Theorem	48
6.2.3	Potential Energy When the Current is Constant	49
6.3	Calculation of the Magnetic Flux	49
6.4	Mechanical Problem Formulation	50
6.5	Equilibrium and Stability	51
6.5.1	Equilibrium Equations. Fundamental Solution	51
6.5.2	Stability of the Equilibrium	52
6.5.3	Critical Loads for the Instability in the v-direction	54
6.6	Numerical Results	55
	Conclusion	57
IV	Appendix	59
A	Demonstration of the Maxwell's Theorem	61
B	Complex Potential Due to a Line Current	63
C	Expression of the Flux Function and its Derivatives	65

D	Variationnal Problem for the Transverse Direction Stability	67
D.1	Problem Formulation	67
D.2	Numerical Determination of the Critical Load	69

Introduction

Part I

Preliminary Study

Chapter 1

Actuation Techniques for RF MEMS

1.1 Electrostatic Actuation

Currently almost all RF MEMS developed use an electrostatic actuation principle. The advantages are obvious: the basic principle is simple (a potential between 2 electrodes creates a force between them), the implementation and fabrication techniques are not too complicated and can be done using surface micromachining. Many switches have been already developed, and a review of these can be found in [1].

I will not discuss here the interest in developing MEMS for RF communications. Suffice to say that RF switches in particular offer electrical characteristics far better than what the best P.I.N. diodes can do. However, some problems still remain that prevent their efficient use, namely reliability problems and the fact that still no good packaging method is available for them. Concerning the first issue, the failure mechanisms for DC-contact switches (i.e. metal to metal contact) are resistive (e.g. degradation of the contact area due to impacts) and due to microwelding, and for capacitive switches, the failure is due to stiction. This stiction is linked to charges that remain permanently in the dielectric and create an electric field strong enough to maintain the moving electrode in the down position. The charging of the dielectric material itself is due to the strong electric field necessary for the reliable actuation of the electrode. An important drawback of these switches is that because electrostatic forces decrease relatively rapidly with distance and because we need air gaps in the up position of $2 - 3 \mu m$ to insure sufficient isolation, the actuation requires high voltages (say around $30 V$), at least for the initial movement of the electrode (note that we can't reduce the spring constant of the electrode too much for reliability issues).

Thus usually, in the down position, the voltage is decreased (typically to $5V$), in order to limit the effect of charge trapping in the dielectric. Moreover, other actuation techniques have been studied to try to overcome in particular the

problem of generating high actuation voltages. As we will see in the following, these actuation techniques do not currently produce results that make them interesting for a practical use.

1.2 Other Non Magnetic Actuation Techniques

Electrostatic Actuation is largely dominant for MEMS switches. Other actuation techniques can be used to avoid the drawbacks of the electrostatic switches, namely the high voltages required.

Hence an electrothermal has been developed for example by the LETI [3], with an actuation voltage of less than $3V$. But the actuation power is in the tens of milliwatts range (compared to no static power consumption for electrostatic switches), and the closure time in the hundreds of nanoseconds, and thus this switch is quite slow.

Another technique that could be employed would be to use piezoelectric actuation, although here again the implementation is more difficult than for the electrostatic case. In the following, we will concentrate our attention on different magnetic actuation principle, with the Microlab switch for example being currently one of the most interesting switches on the market.

1.3 A Magnetic Switch

In general, we take switches as examples since the actuation principle can then be used for other MEMS structures, like varactors, filters, oscillators, etc... There are of course some additional subtleties like for e.g. the possibility of using the inherent voltage-electrostatic force non linearity for direct filtering+mixing [2], but these can be omitted in this general discussion. In the following, we discuss another actuation principle, which is relevant for the rest of the report, namely by presenting some characteristics of the magnetic switch produced by Microlab [4], [5]. Table 1.1 presents the characteristics of the latching relay. Comparing with the electrostatic switches, we can make a few remarks:

- First, the operating voltage can be maintained low ($< 5V$), but at the expense of high currents in the coil (around $100mA$). The switch can retain a down position thanks to the magnetic field created by a permanent magnet, therefore no external power is needed for latching.
- the switch is slow. The main reason is that a thick ($\approx 20\mu m$) film of permalloy has to be deposited to form the movable part; therefore the mass is important and this slows down the mechanism. With a switching time reported in the order of $500\mu s$, this switch remains very slow for RF systems where typically electrostatic switches change state in about $5\mu s$, and are still slow for practical applications.

From this discussion about different already demonstrated actuation techniques, we would like ideally to use a magnetic actuation because we do not

Table 1.1: Characteristics of the Latching Micromagnetic Relay developed by Microlab.

Characteristic	Reported in [5]	Reported on Website [4]
Operating Voltage	$\approx 5V$	$< 2 V?$
Switching Current	$79 mA$	$< 100 mA$
Switching time (off \rightarrow on)	$0.5 ms$	-
Switching current pulse	$< 0.2 ms$	$< 0.1 ms$

want to generate high operating voltages, but also low currents for a low power dissipation (comparable to diodes, ideally in the μW range, since electrostatic switches dissipate virtually no DC power). Therefore a natural conclusion is that the main magnetic field has to be created with permanent magnets, and not with a coil. Because of the constraints on the switching time, the movable structure must remain small, excluding the usually used thick NiFe structures. The idea, to be presented in the following, is simply to create a strong permanent magnetic field, and actuate a structure placed in this field using Lorentz (more precisely Laplace) forces, by feeding a small current through the structure. Therefore the movable structure can remain small, even smaller than in the electrostatic actuation case. In fact, the idea is so simple that if it has not been demonstrated so far, it is mainly because good permanent magnets (hard magnetic materials) are not easily obtained at the microscale by standard deposition techniques. Therefore, before presenting our design further, it is necessary to review the current state of available magnetic materials for MEMS.

Chapter 2

Magnetic Materials for MEMS

2.1 Overview

We will deal in the following with two types of magnetic materials: soft and hard. An introduction to the properties of these materials can be found in chapter 4. Soft magnetic materials have been used and integrated into MEMS technology for some time now ([10],[11]). Hard Magnetic Materials are subject to an intensive research work dealing with very thin films of these materials for applications in memories. But the literature on thick films of hard magnetic materials is rather limited, although the applications in MEMS are today considered. Typically, we hope to have hard magnetic materials (i.e. permanent magnets) with the best characteristic possible in order to create a strong magnetic field. This should allow us then to obtain strong Lorentz forces with low current and power dissipation.

Some groups, essentially interested in the physics of these films, reported thick films of rare-earth permanent magnets before 1990 ([6], and [8] for a more recent publication). The properties of these films are actually good and sufficient for our design. The possibility of integrating them into a process remains an issue. These films were obtained by sputtering and needed that the substrate be heated at a temperature of more than $600^{\circ}C$. The process has to take this high temperature step into account.

There is of course a strong interest in depositing permanent magnets through more easily integrated techniques such as electroplating [14]. The set up in this case is simple, but unfortunately, the properties reported ([16]) are not sufficient if we want to bias a magnetic circuit and use a reasonable amount of power for the actuation (the properties are approximately 10 times worse than for the sputtered magnets).

2.2 Current State

2.2.1 Research Groups

Serial Fabrication

In this paragraph I include the reported systems for which the fabrication is not parallel: that is, the magnets are manipulated individually. This is not what we would like (not compatible with an industrial process), but could be use for demonstration.

- **Possibilities at the university of Michigan:** it seems to be difficult to develop a process involving permanent magnet materials at the SSEL. Prof. Gianchandani has already worked with permanent magnets when he was a professor at the University of Wisconsin-Madison but apparently was not willing to cooperate. Suffice to say that they used micro-electro-discharge machining to shape NdFeB magnets.
- **Laboratoire d'électrotechnique de Grenoble, France:** Dr. Cugat's group. They have also developed a movable mirror using magnets ([20]), for which they glued micro magnets provided by Comadur, a swiss company. They do not report the thickness of these magnets. They are more or less collaborating with the team of prof. Kornilov ([8]) and cite his work about the 300 μm thick films of NdFeB. They also reported a permanent magnet micromotor [21]: the integration of the SmCo magnets is not clear, and the work of Kornilov is the only work on thick hard magnetic films cited again. They also work in Grenoble with the CEA-LETI, and I contacted there Dr. Gaud, director of the magnetic actuators department in August 2002. They seemed to be still trying to obtain satisfying results for electrodeposited magnetic films, and he told me that basically all possibilities should be considered in this field.

Magnetic Films for Batch Fabrication

- **Queen's College of New-York:** Dr. Cadieu [6]. This is the first report that I found on thick films of hard magnetic materials. Thick films of SmCo are sputtered with and good magnetic properties. Drawback: the substrate has to be heated. Cadieu worked on several projects intended to integrate these films in MEMS. An example is [7], where a 25 μm thick Sm-Co film is used to bias Ni-Fe permalloy films. This last reference is interesting for different reasons: it gives the condition used for sputtering Sm-Co (and Ni-Fe also in this case), and shows a sandwich configuration with hard and soft magnetic material, although they use a thick dielectric layer between the two films in this case. The way they create their sandwich structure is not reported.
- **Moscow State Institute of Steel and Alloys:** Dr. Kornilov [8]. Very thick sputtered magnetic films of NdFeB are reported, up to 300 μm .

Excellent magnetic properties. Again the substrate has to be heated, around $500^{\circ}C$. Very few information about this group is available.

- **Nagasaki University, Japan:** [9]. Good properties, the laser ablation technique achieves better deposition rates ($50 \mu m/hr$) than sputtering, but annealing at $923 K$ again.
- **M. Allen and L. Lagorce:** [12], [13]. They have developed polymer magnets, that is resin-bonded magnet films. The magnetic properties reported so far are not as good as for the sputtered magnets ($B_r \approx 0.3T$ and $B H_c \approx 350 kA/m$), but the possibilities to integrate them in MEMS processes are very interesting. This article should be reviewed in detail; moreover, it should be possible to increase the magnetic properties of these magnets (see discussion in [18]).
- **Other groups and techniques:** i put here together some interesting works from other groups, but none of them fulfill our requirements. They represent however a trend towards an easier integration of the deposition of magnetic materials with MEMS processes. There are reviews of magnetic materials for MEMS by Judy ([17], [16]) and Chin ([18]). Co-Pt and Fe-Pt are good futur candidates for MEMS because they should be adapted to electroplating; see for example [23] for electrodeposited Co-Pt, although the thickness is only $0.2 \mu m$. Ahn ([14]) has also already used electroplated permanent magnets in actuators, but the properties of his magnets are not sufficient for our purpose.

Christenson, Garino and Venturini at Sandia National Labs hold a patent on the batch fabrication of precision miniature permanent magnets, but i cannot currently get the paper that i give as a reference [15].

2.2.2 Companies

There is very little information that i can provide in this section.

Micro magnets

If we need to use small magnets that we want to manipulate individually, we should be able to get them from the companies that provide micro magnets for the watch industry. Cugat describes such a process in [20]. They glued and micromachined the magnets (Sm-Co type). However the final dimensions are not reported, so the size for our design might not be compatible. The magnets were provided by Comadur ([26]), which is a swiss company. There is probably a company in the US providing these magnets, but i could'nt find it.

Deposition of magnetic films

Only very few companies give information about the possible deposition of magnetic materials. **San Diego Magnetics** ([27]) deposit thin films of magnetic materials with different techniques and works in the field of MEMS although the thickness seems to be limited to $15 \mu m$. This is the most interesting company for our purpose that I found.

Us, inc. ([28]) sells sources for planar magnetron sputtering that they say compatible with Nd-Fe-B, but probably don't deposit the materials themselves. The Materials Science and Technology Division of the Naval Research Laboratory put on its web page that they have a magnetic materials MBE system, but without further explanation ([29]).

In general, we will probably not find on a website the exact configuration that we need. Given than the use of these hard magnetic materials is emerging at this scale, especially with this thickness, we have to find a company which would be interested in trying to deposit with the specification that we need. I just think that because we do not ask a standard material, thickness, and process, we cannot find this information by just consulting the adds or even the basic information given on the websites of the companies. Basically we will need to proceed by trial and error because we don't know what can really be done.

Chapter 3

Microsystems Actuated by Lorentz Forces

3.1 Introduction

We are trying to obtain magnetic actuation without burning too much power. A design will be proposed in the following which intends to create a high magnetic field density at no cost with a permanent magnet material and a soft magnetic material to concentrate the flux. The process proposed will be a batch fabrication process, instead of attaching individual magnets to the chip.

For the moment, we will assume that we are able to create a magnetic field density of $1T$ in the direction perpendicular to the substrate. We consider some possible applications and related issues in the following sections.

3.2 Switches

We have briefly discussed in chapter 1 the disadvantages associated with electrostatic actuation. An important characteristic of these forces however is that the electrostatic force in the down position is strong, allowing low contact resistance and keeping the contact without dissipating any DC power. The expression of the electrostatic force is simply:

$$F_{el} = \frac{\epsilon_0 AV^2}{2(d + \frac{t_d}{\epsilon_r})^2} \quad (3.1)$$

with A the area of the electrodes, V the voltage between the electrodes, d the air gap height, t_d the dielectric thickness and ϵ_r the dielectric relative permittivity. When the contact is made, we can compute the force between the electrodes by the expression:

$$F_{el,down} = \frac{\epsilon_0 AV^2}{2(\frac{t_d}{\epsilon_r})^2} \quad (3.2)$$

This force is distributed over the area of contact. Consider now a beam with a current i_e through it, and placed in a strong magnetic field B . The lineic force acting on the beam is $i_e \times \mathbf{B}$ and therefore when the contact is made, the total force applied to the bottom electrode will be, assuming the current and the magnetic field are perpendicular:

$$F_{m,down} = i_e B c \quad (3.3)$$

where c is the length over which the contact is made.

To have a sufficiently low resistance in the on position, the contact force on most metal-to-metal contact series switches should be at least $100 - 200 \mu N$ [30]. For the electrostatic actuation, if we suppose that we deal with a beam $5 \mu m$ wide, that the contact can be made on a length $100 \mu m$, a dielectric with $t_d = 0.15 \mu m$ and $\epsilon_r = 7.6$, a voltage $V = 5 V$, then we get $F_{el,down} = 142 \mu N$. The calculation for the magnetic force gives: $F_{m,down} = 1 \mu N$ only for a current of $10 mA$, and thus we see that using the Lorentz force is impractical for maintaining the contact. However, the advantage of this force is that it is independent of the gap with the substrate, and thus we could use it to actuate the structure, and then maintain the contact by applying a small voltage. Moreover, by reversing the current, we can obtain a force in the opposite direction which could be used in case of stiction of the beam to separate it from the substrate, and hence enhance the yield and also reliability of the switch. Using Lorentz forces for yield enhancement has already been considered in [31].

3.3 Voltage Tunable Capacitor

Voltage Tunable Capacitors have application in voltage controlled oscillators. There is not much to say about this since we can use basically a capacitive switch to obtain high capacitance ratio. Diodes are still used in LC-oscillators, where the capacitance of a reverse biased pn-junction can be controlled by the bias voltage:

$$C_{var} = \frac{C_0}{\left(1 + \frac{V_r}{\Phi_b}\right)^m}, \quad m \approx 0.3, \Phi_b \approx 0.7V \quad (3.4)$$

One disadvantage of the diodes is that the range of variation of the capacitance is limited. For a variation of V_r from $0V$ to $3V$, C_{var} varies from C_0 to $0.6 C_0$. On the contrary, good electrostatic switches can today achieve a ratio of more than 100 [33].

3.4 Filters

One of the most interesting applications in the utilisation of a high magnetic field could be to obtain filters with a higher resonant frequency compared to the ones obtained so far using electrostatic actuation (eg. [2]). The principle was already studied in [34]. In order to increase the resonant frequency of the

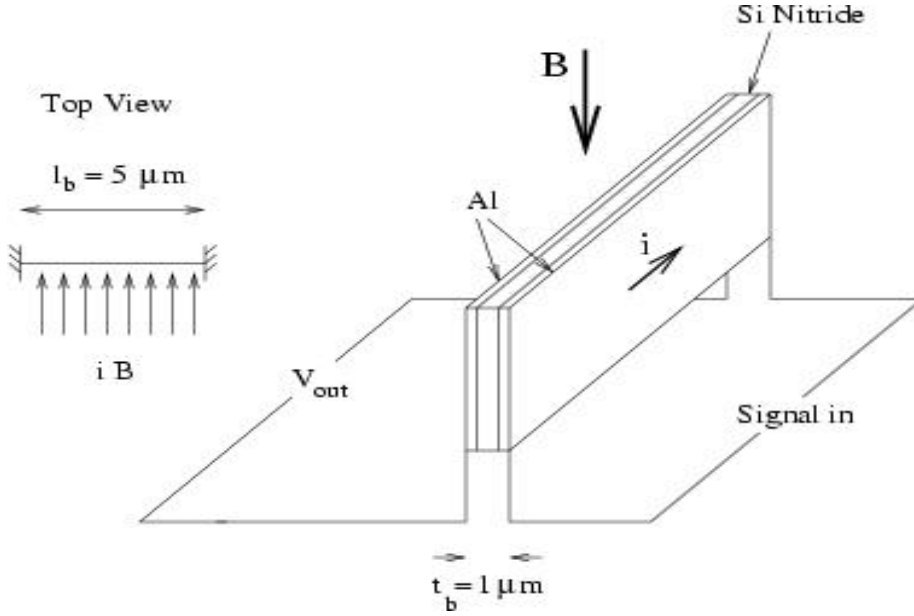


Figure 3.1: Vibrating clamped-clamped beam in a high magnetic field.

vibrating beams, the length has to be decreased: the dimension might become too small to keep the electrostatic actuation principle (with an electrode under the vibrating beam).

As an example, I will take a simple system: suppose we have in the magnetic field a short clamped-clamped beam, composed of three layers: $Al/Si_3N_4/Al$ (see figure 3.1). This should be quite easy to fabricate compared to the refined process used to obtain free-free beams for example. Let us use the equations derived in [34] for the beam fixed at both ends, in the case where we neglect the intrinsic stress.

Resonant Frequencies of the beam:

$$f_{n,b} = \frac{\eta_{n,b}^2}{\sqrt{3}\pi} \sqrt{\frac{E}{\rho}} \frac{t_b}{l_b^2} \quad (3.5)$$

with $\eta_{1,b} = 2.365$, $\eta_{2,b} = 3.927$, $\eta_{3,b} = 5.498 \dots$ Assuming the dimensions given on the figure, and taking $E \approx 385 \text{ Gpa}$ and $\rho \approx 3.1 \text{ gm.cm}^{-3}$ as if the beam was only made out of silicon nitride, we get for the first resonant frequency $f_{1,b} \approx 458 \text{ MHz}$ (the highest resonant frequency obtained with free-free beams in [2] was 92 MHz).

The principle of the system is to drive the beam with an input current i (which creates a variable Lorentz force due to the presence of the B field) and to read the output using a separate path where a voltage is created due the the fact that we have a circuit moving in a magnetic field:

$$V = \oint (\vec{v} \times \vec{B}) \cdot d\vec{l} \quad (3.6)$$

where \vec{v} is the velocity of the segment of the conductor $d\vec{l}$. If we integrate along the mode shape of the lowest harmonic (note also that the even modes cannot be detected), we obtain $V = 3.287 l_b f B u_{mp}$, where u_{mp} is the maximal deflection, at the midpoint. We can obtain, in general:

$$u_{mp} = \frac{i B l_b^4}{32 E w_b t_b^3}$$

But at the resonant frequency, this value is multiplied by Q , where Q is the quality factor of the mechanical system, linked to the damping. A mechanical Q of the order of 10000 should be feasible, possibly under vacuum conditions (see [2]). We finally get:

$$V_{resonance,rms} = 3.287 l_b f_{1,b} B \frac{i_{rms} B l_b^4}{32 E w_b t_b^3} Q \quad (3.7)$$

Suppose $i_{rms} = 2 \text{ mA}$ (take $R_{beam} \approx 1 \Omega$ for the power consumption), then we obtain $V_{induced,rms} = 7.64 \mu V$, if $Q = 10000$.

3.5 Impossibility of Mixing

An interesting possibility of the resonant structures electrostatically actuated is that we can perform at the same time filtering and mixing [2]. It is important to note that this feature is possible due to the nonlinearity of the force with respect to the input signal, namely the fact that F is proportional to V^2 . Therefore if the input is some $V_{lo} + V_{rf}$, the force will have components at frequency $rf - lo$ due to the term $V_{lo} \times V_{rf}$ and we can design the system so that this latter frequency coincides with the resonant frequency of the beam.

In the case of the Lorentz force, nothing similar is possible since the force is linear in the input signal i_e .

Part II

Design of a Magnetically Actuated Switch

Chapter 4

Design of the Magnetic Circuit

4.1 Introduction

So far we have assumed that the structures considered were moving in a strong magnetic field of 1T, parallel or perpendicular to the plane of the wafer. The way we create the magnetic field is of course of high importance, and it is even questionable if such a high magnetic field can practically be reached. In this chapter, we recall the fundamentals of magnetic circuit design and present simulations showing how we could create the magnetic field. Two configurations are considered, creating the magnetic field either in the vertical or horizontal direction. Some considerations are made on the fabrication processes, using the information given in chapter 2. Finally, a study has been conducted for the horizontal field configuration on the influence of air gap losses on the biasing of a thin magnetic circuit.

4.2 Magnetic Circuit Design

4.2.1 Overview

The magnetic circuit considered will be composed of a permanent magnet creating the magnetomotive force, a core made out of a soft magnetic material with high permeability (such as permalloy NiFe) to conduct the magnetic flux, and an air gap, in which we can place a beam to be actuated (see fig. 4.1).

For a permanent magnet in a magnetic circuit, a demagnetizing field inside the material is produced by, and is in opposite direction to its own magnetization [35]. H_m in the material is in the opposite direction to B_m , therefore we are interested in the second quadrant of the hysteresis loop of the curve B-H, called the demagnetizing quadrant.

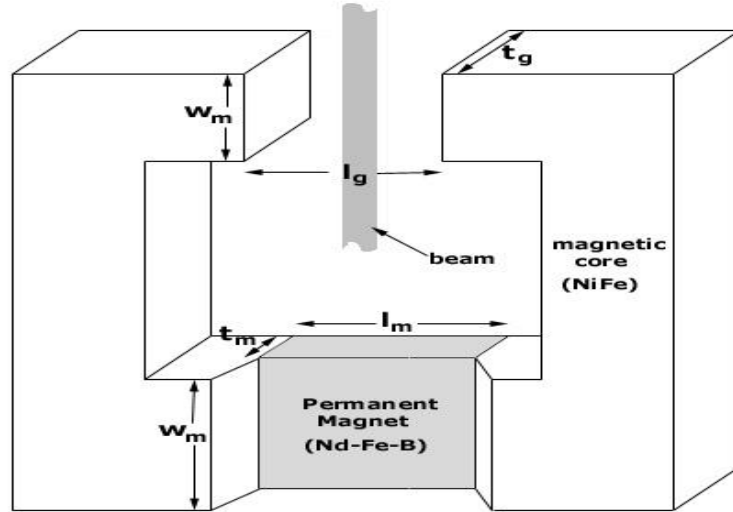


Figure 4.1: Typical magnetic circuit, with dimension labels.

An example of a demagnetizing curve is given on fig. 4.2. The important quantities are the remanence B_r (when $H = 0$), the flux coercivity BH_c , and also important is the maximum of the energy product $(BH)_{max}$ corresponding to the point on the curve on which we want to work, for reasons that will appear clear in the following. The coercivity is a measure of the resistance of the permanent magnet to demagnetization, and we want to have it as large as possible.

4.2.2 Equations

Considerations on the quality of the permanent magnet and soft magnetic material will be given in the following sections. Let us concentrate here on the determination of the different (minimal) dimensions in order to create a field of 1T in the air gap. The numerical values used in these section for illustration purposes will be reviewed later in the case of microfabricated magnetic materials, but the equations will remain the same.

First note that the magnetic circuit doesn't work ideally because of magnetic reluctance of the magnet and soft iron, and because of flux leakage in the air gap. The design of the circuit is controlled by three basic equations, in a form which accounts for these leakages:

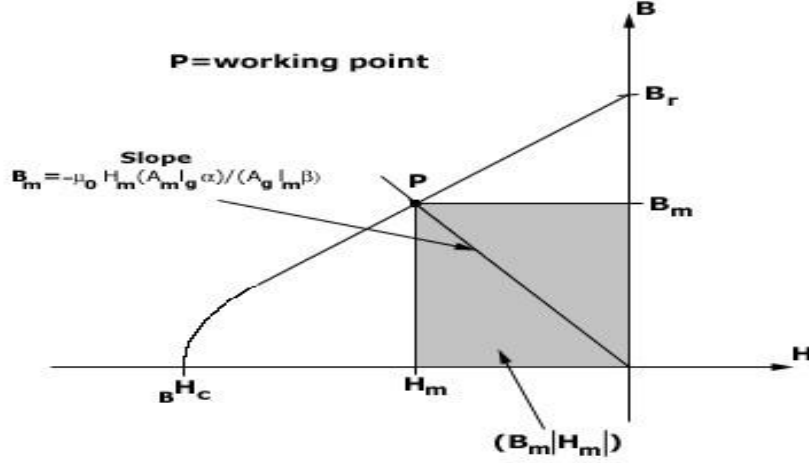


Figure 4.2: Demagnetizing curve for a permanent magnet material.

$$H_g l_g = -\alpha H_m l_m, \alpha \leq 1 \quad (4.1)$$

$$B_g A_g = \beta B_m A_m, \beta \leq 1 \quad (4.2)$$

$$B_m \text{ and } H_m \text{ are on the demagnetizing curve} \quad (4.3)$$

In the following we take $\alpha = 0.9$ and $\beta = 0.7$, values that give good agreement with the simulations for typical magnetic materials. H_g and H_m are the magnetic field intensity in the air gap and in the permanent magnet, B_g and B_m are the corresponding flux densities, A_g and A_m are the cross section areas of the air gap and the permanent magnet ($A = t \times w$).

We can note the importance of a high coercivity for the material. We need

$$|H_m| = |H_g \frac{l_g}{l_m}| < |B H_c|$$

If we want $H_g = 1T/\mu_0 = 7.96e5 \text{ A/m}$ in the air gap, a constraint exist on the ratio l_g/l_m because a medium performance Nd-Fe-B material for the permanent magnet typically has a coercivity of only $5e5 \text{ A/m}$, and in our case a deposited magnet will have properties which are far from these numbers. However in practice, there will be other more restrictive constraints and this one should be verified in general.

We are free to choose the working point we want on the demagnetizing curve. A common practice is to choose the point that allows to create the magnetic

field in the air gap using the minimum volume of magnet possible. Multiplying equations (4.1) and (4.2), and with $V = A \times l$, we obtain:

$$(V_m)_{min} = \frac{\mu_0 H_g V_g}{(B_m |H_m|)_{max}} \quad (4.4)$$

Therefore we see that we should work at the point of the demagnetizing curve where the energy product is maximal. A good approximation for a first design is to consider that this point corresponds to $B_m = B_r/2$ and $H_m = H_r/2$, as if the demagnetizing curve was a straight line.

Once we have chosen the desired working point, we note that we must also lie on the line:

$$B_m = \mu_0 |H_m| \frac{A_g l_m \alpha}{A_m l_g \beta} \quad (4.5)$$

Fixing the ratio:

$$\frac{l_m A_g}{l_g A_m} = \frac{B_m \beta}{\mu_0 |H_m| \alpha} \quad (4.6)$$

Example: suppose we have a hard magnetic material with $|B H_c| = 520 \times 10^3 \text{ A.m}^{-1}$ and $B_r = 0.8 \text{ T}$. If we consider that we need $H_g = 800 \text{ kA.m}^{-1}$ in the air gap, we have:

$$\begin{aligned} \frac{l_m A_g}{l_g A_m} &= 0.95 \\ \frac{l_g}{l_m} &= \alpha \frac{|H_m|}{H_g} = 0.292 \\ \frac{A_g}{A_m} &= 0.292 \times 0.95 = 0.28 \end{aligned}$$

And usually the dimensions of the air gap are fixed by the application, fixing then the dimensions of the magnet.

4.3 Planar Configuration

4.3.1 Presentation of the Design

A first straightforward implementation for a capacitive switch is shown on fig 4.3. For this, we need to move current carrying beams upwards or downwards, and so the generated magnetic field should be parallel to the plane of the wafer. Therefore, the beams would be placed in the air gap of the magnetic circuit shown on fig. 4.4. This magnetic circuit would have to be deposited on the wafer, and obviously the dimension that poses the biggest fabrication problems is the thickness.

It is quite easy to control the width and length of the magnet as soon as we have a mean for shaping it, but as we have seen in chapter 2, depositing thick hard magnetic material with good properties is not an easy task. Moreover, the

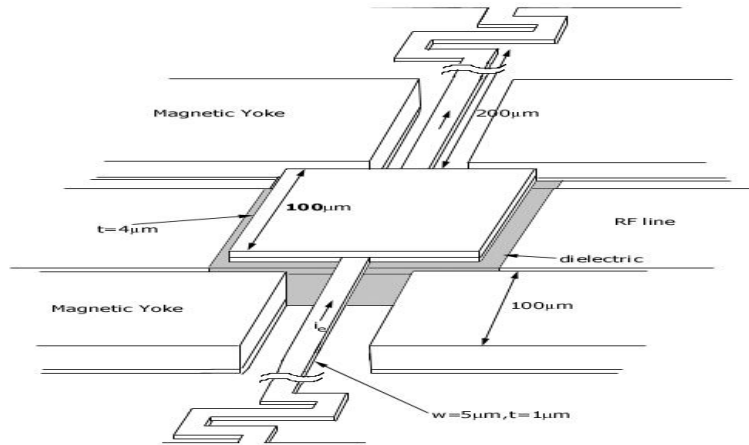


Figure 4.3: Capacitive switch actuated with the Lorentz force on the beams.

process integrating the switch structure and the magnetic circuit would have to be carefully studied. Quite often, the deposition of the hard magnetic material requires a high temperature step, impossible if the Aluminum switch has already been deposited. On the other hand, if we deposit a thick magnet first, then we can't approach the mask close enough to the wafer to shape fine features. But we have to control the width of the beam precisely, to have a width for the air gap then as small as possible. Typically the width of the beam would be of the order of $5\mu m$, the width of the air gap $15\mu m$.

A solution to these problem could be to use a transfer process similar to the process used for the RF switch of the Berkeley sensor and Actuator Center [36]. The principle of this process for our case, shown on fig. 4.5, would allow the independant fabrication of the magnetic circuit on one wafer and the movable structure on the other wafer. The alignment at the bonding step need only to be done in such a way that the beams fall in the air gap. The main difficulty that this process currently encounters is to obtain a repeatable height for the switch structure with respect to the bottom electrode. Since in our case, the force would be independant of the distance between the capacitive plate and the substrate, we would still be able to operate a switch positionned too high by giving a reasonable additional amount of current. No precise study of this process was carried during this project, but I think it might be a reasonable idea to consider. The advantage of keeping a planar configuration is that it allows to maintain the contact with a strong electrostatic force thanks to the large area of the suspended capacitive plate.

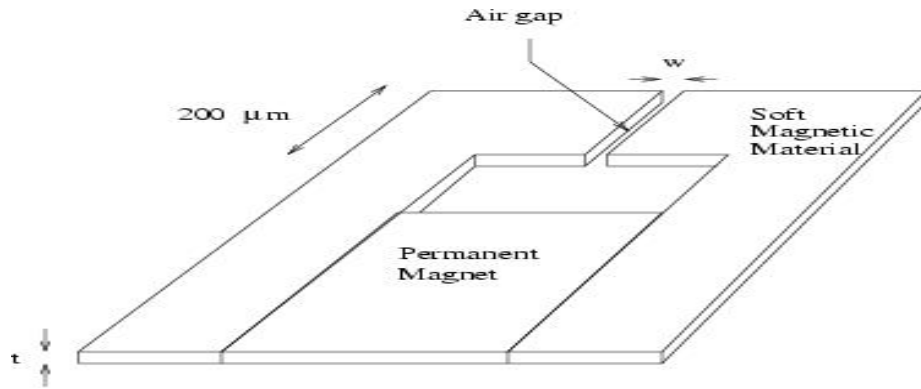


Figure 4.4: Planar magnetic circuit.

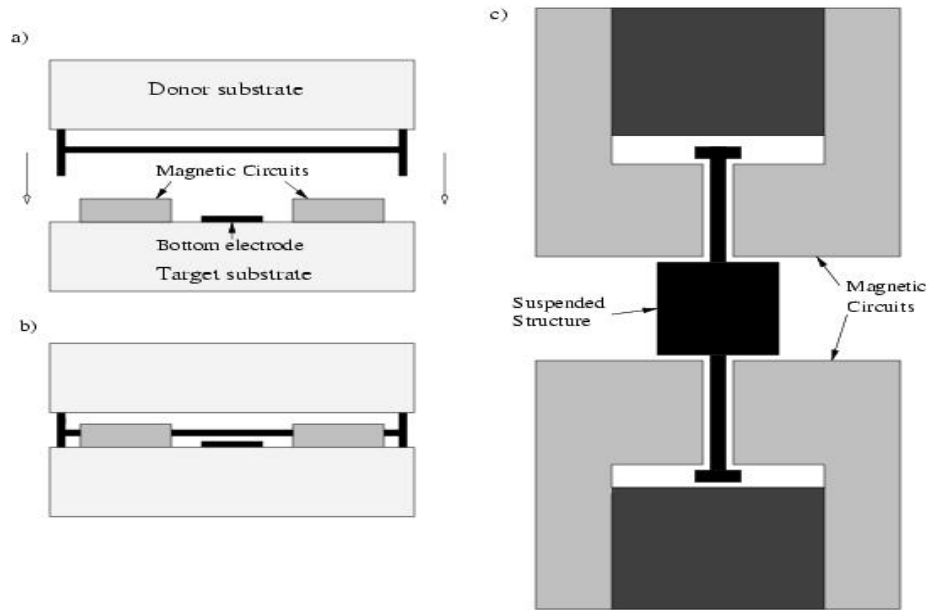


Figure 4.5: Process for the magnetic switch in the planar configuration, using the Berkeley Transfer Process. The final top view is shown on c).

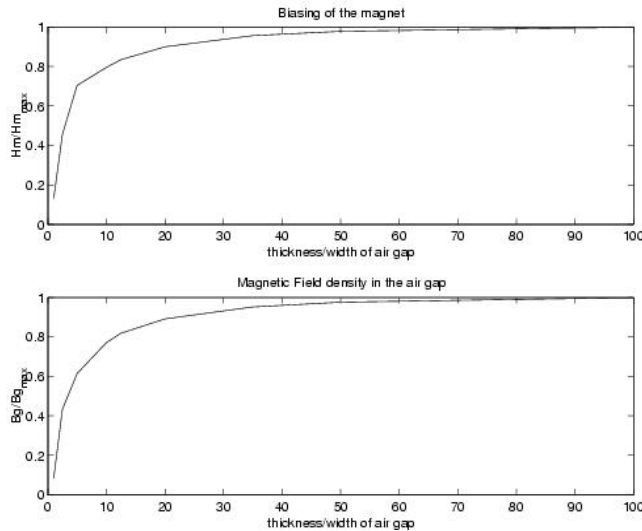


Figure 4.6: Influence of thickness on the working point of the magnet and the field in the air gap. We see on the right the asymptotic behavior corresponding to the value calculated analytically. The ration t/w needs to be quite high to reach this behavior.

4.3.2 Impact of the Thickness on the Biasing of the Magnetic Circuit

As we mentionnes previously, the thickness of the planar configuration of the magnetic circuit is critical. A limiting factor to the magnetic field density in the air gap is the ratio t/w , thickness of the magnetic circuit over length of the gap (see fig. 4.4 - note that here w represents what we called in a previous part l_g). We performed a numerical study of the influence of this parameter on the field in the air gap, whose principal results are summarized on fig. 4.6. These results allow us to determine when the derivation done in part 4.2.2 are valid to compute the magnetic field in the air gap.

- When the ratio t/w becomes too small (typically here, the ratio is 1, $20\mu m$ thick for an air gap $20\mu m$ wide), the fringing fields increase a lot and an additional factor is that it changes the working point of the magnet. The equivalent area in the middle of the air gap used in the analytical calculation becomes very large. What the finite elements simulation predicts, is that **it becomes impossible to bias the permanent magnet at the right point** (cf. previous discussion), that is, it predicts that the magnet remains at a point H_m quite small instead of having H_m in the order of $H_c/2$ as we wanted.
- Figure 4.6 shows the influence of the thickness on the magnetic character-

istics of the circuit. Ideally, without taking the fringing fields into account, the magnetic field in the magnet and in the air gap should be independent of the thickness. We see that for ratios t/w in the order of 40 or greater, this is true. But we see that we cannot make this assumption for a ratio of 1. And the problem is not just a leakage problem which could be solved by increasing the dimensions of the magnet. I tried to use the analytical dimensions obtained to get a B in the air gap around $10T$, to see if the simulation would predict something 10 times less, that is, in the order of $1T$, but this doesn't work better than with a magnet with realistic dimensions. The main reason is probably again that the losses have an influence on the conservation of the flux and the Ampere Law, and the result is that the magnet is not working properly.

- This is not just a problem of calculation or bad mesh. In [37], the same ratio of 1 for the thickness and width is used in the fabrication of a soft magnetic material with an air gap, and the result of the experiment differs from the calculation by a factor of 10 also.
- So the result obviously depends on the thickness, and for this planar magnetic circuit, a 3-D analysis is required. With a thickness of $20\ \mu m$ and width of the air gap $20\ \mu m$, I was not able to have a field in the air gap of more than $0.2T$, even with a very large magnet. When the thickness increases more, the magnet begins to work properly and we can have the behavior predicted by the analytical result. I would say that a ratio of 2.5 to 5 would be needed to get relatively good results. We reach the limitation of the thickness due to the electrodeposition step, if the width of the air gap is $20\ \mu m$.

4.4 Vertical Configuration and Packaging

An alternate configuration was considered, which creates a magnetic field perpendicular to the plane of the wafer. It consists of a stack of hard and soft magnetic materials, and integrated the packaging in the fabrication process. This section presents a complete design including considerations on the process.

We study here the particular design in the case we would use the permanent polymer magnets obtained by Mark Allen at Georgia Tech (Strontium Ferrite/Polyimide Composites), with the properties reported. The advantage of these magnets would be that they are more compatible with micromachining and MEMS processes than sputtered magnets.

The magnets have less good properties compared to what we considered so far, so this design needs a bigger magnet. But we see here how the structure of the magnetic circuit compensates the lack of good properties to achieve a high magnetic field in the air gap.

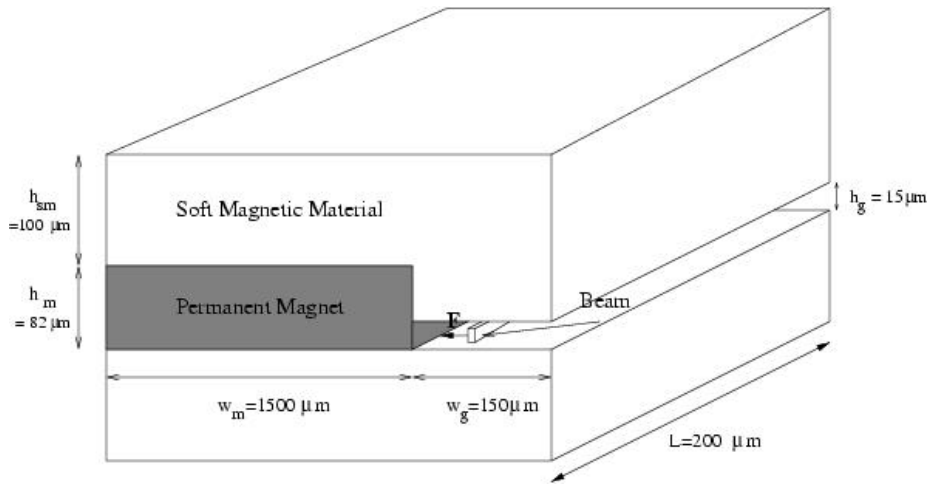


Figure 4.7: Final device with dimensions.

4.4.1 Final Device

Figure 4.7 presents the final cross section of the device we would like to obtain. The movable part is a beam, which will be terminated by a capacitive plate for example, or more probably just used directly to make a DC contact. We want to actuate this beam in the horizontal direction: it is suspended inside the airgap of the magnetic circuit, and thus in a region where a strong vertical magnetic field exists. When a current goes through this beam, a horizontal Lorentz force is created. The next section shows how this vertical stack might be done.

4.4.2 Process

Figure 4.8 presents the possible process flow that we imagined. This process requires two bondings to enclose the movable structure inside the air gap of the magnetic circuit. An alternative would be to use only one bonding step for the top magnetic yoke if we see that it is possible to deposit (or screen-print) the permanent magnetic material on top of the soft magnetic material, or even not to use any bonding if the top soft magnetic material can be electrodeposited with enough thickness on top of the structure. See figures 4.9 and 4.10 for these variations. Note that in the last case, the thick permanent magnet material has to be deposited after the structure, otherwise we won't be able to define the dimensions of the movable beam ($1\mu\text{m}$ wide, $5\mu\text{m}$ thick) with enough precision.

4.4.3 Magnetic Characteristics of the Materials

- Hard Magnetic Material

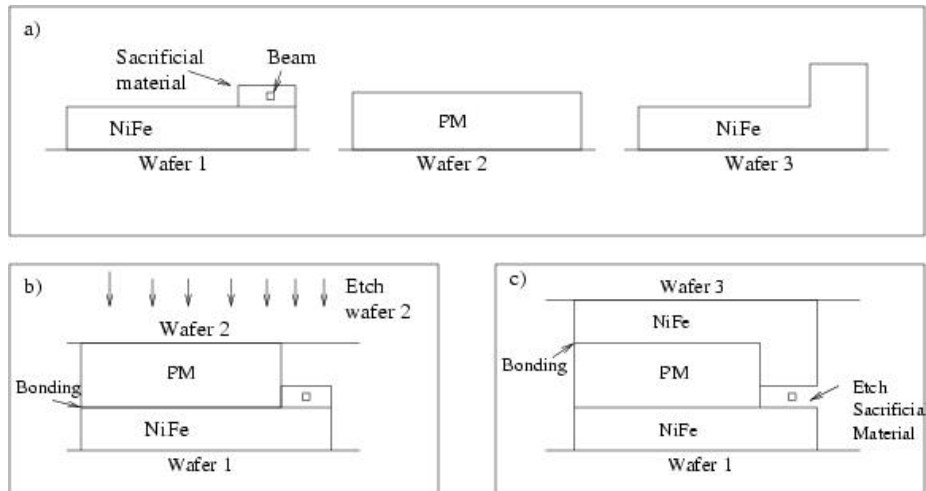


Figure 4.8: Possible Process flow with two bonding steps.

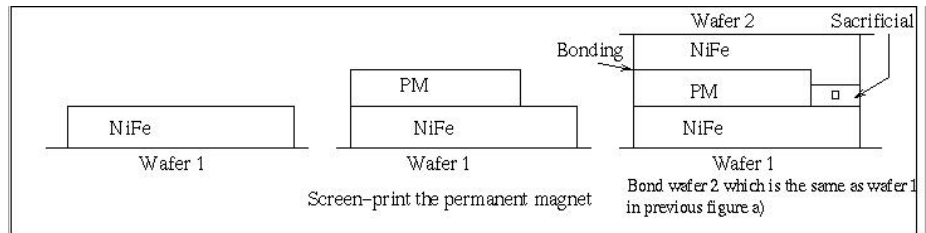


Figure 4.9: Possible Process flow with one bonding step and screen printing of the magnet.

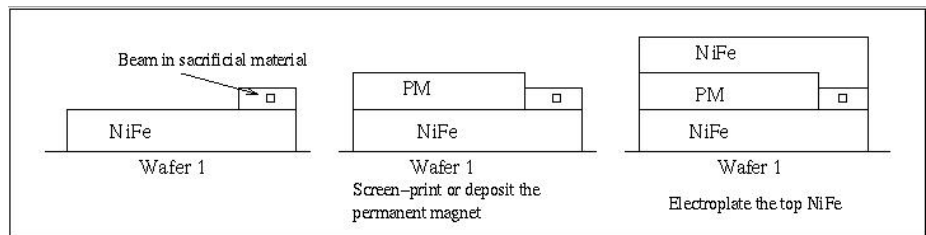


Figure 4.10: Possible Process flow with electroplating of the top soft magnetic material. The magnet has to be deposited after the movable structure.

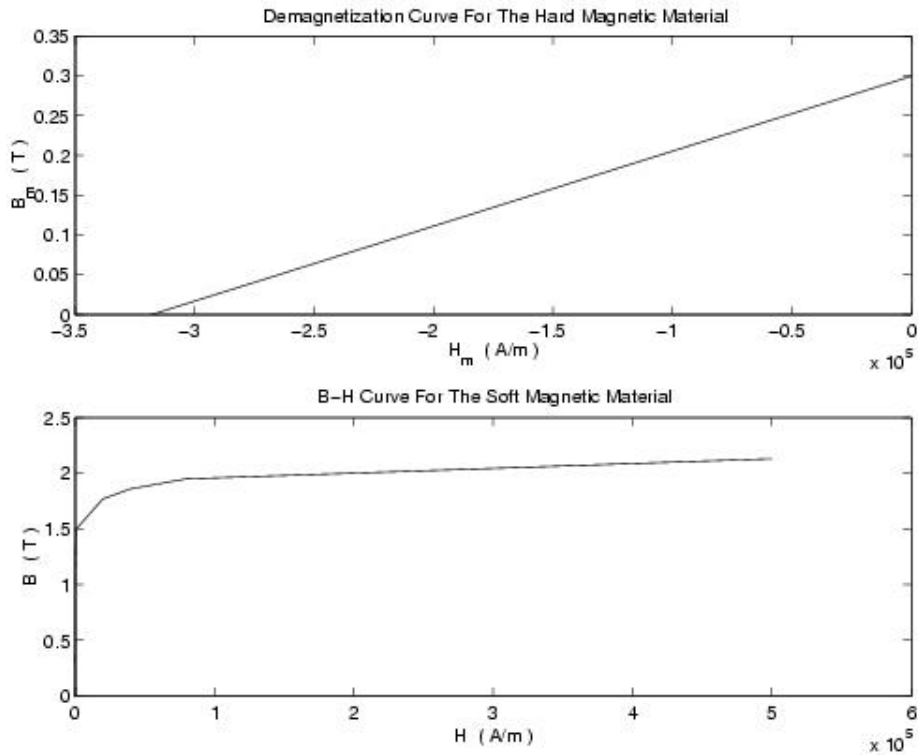


Figure 4.11: B-H Curves for the hard and soft magnetic materials.

Figure 4.11 presents the demagnetization curve we used in the magnetic simulation for the hard magnetic material. This is an idealized curve with coercivity and remanent field values extracted from [12]. $BH_c = 318 \text{ kA/m} \approx 4000 \text{ Oe}$ and $Br \approx 0.3T$. Note that the direction of magnetization has to be the vertical direction (perpendicular to the wafer).

- **Soft Magnetic Material**

The information for the (electroplated) soft magnetic material is extracted from [10]. Coercive force = 47 A/m , saturation magnetization $M_s = 1.5 \text{ T}$ and relative permeability $\mu_r = 4500$. The BH curve obtained is also given on figure 4.11.

4.4.4 Magnetic Simulation Results

With all the elements presented, the simulation of the magnetic circuit gives a vertical magnetic field density of approximately 1 T in the air gap, which agrees with the preliminary hand calculation. The dimensions should be corrected once we have the exact characteristics of the materials, for example to bias the

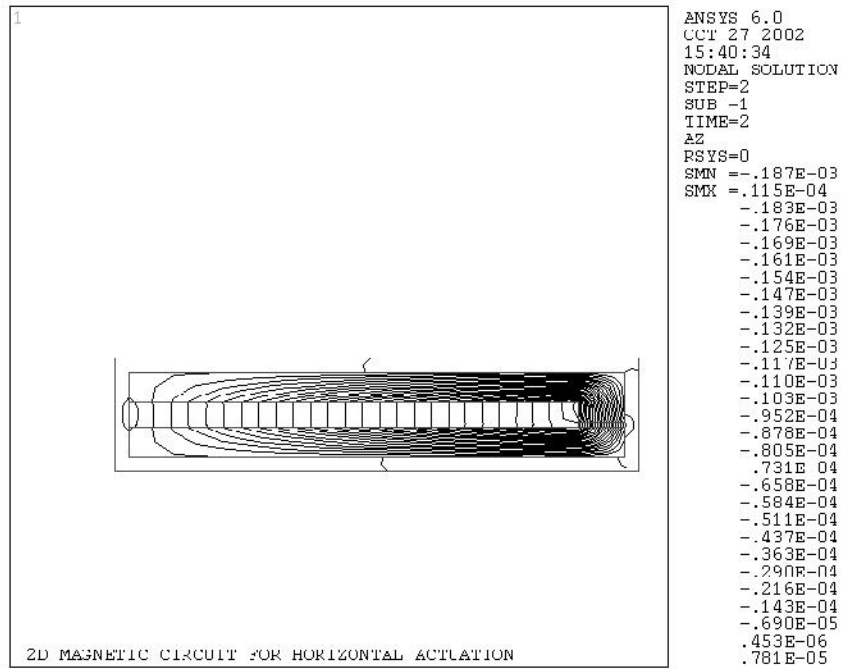


Figure 4.12: Distribution of the flux lines in the magnetic circuit.

magnet at the $(BH)_{max}$ working point. But in general, the circuit behaves well (in particular doesn't suffer from the leakage problems in the air gap which prevented previous designs to work because of biasing problems in the magnet).

Chapter 5

Mechanical Analysis

5.1 Overview

This chapter presents a compilation of various simple mechanical studies we have done on the mechanical systems involved. Here we assume generally that we are able to place our structures in a magnetic field intensity of 1 T , as discussed in the previous chapters, and we evaluate some important characteristics of the structures we could use as RF components (mainly switches). Among these characteristics are power consumption, contact force issues, switching speed, maximal displacement (to allow a good isolation in the open state), etc. The chapter is divided into two parts: static and dynamic analysis. To be added in the future is a part on contact mechanics and the problem of contact resistance build-up for DC metal-metal contact switches, which is still a major issue in RF MEMS switches.

Note that this part cannot provide definitive results, since we still lack at this point a completely realistic design confirmed by experiments in the fabrication laboratory. Therefore the numerical examples included are simply given as references.

5.2 Static Analysis

5.2.1 Bending of a Beam Subjected to a Uniform Load

The equation governing the static equilibrium of the beam is:

$$\frac{d^4 z}{dx^4} = \frac{i_e B}{EI}, \quad x \in [-L, L] \quad (5.1)$$

where z is the vertical displacement of the beam at the horizontal position x , $2L$ the length of the beam, E is the Young's modulus of the material, I is the modulus of inertia ($I = wt^3/12$ for a beam with width w and thickness t), i_e is the current in the beam and B the magnetic field density.

We add the following boundary conditions, depending on the way the beam is attached:

$$z(-L) = z(L) = \frac{dz}{dx}(-L) = \frac{dz}{dx}(L) = 0 \quad (\text{Clamped} - \text{Clamped Beam}) \quad (5.2)$$

$$z(-L) = z(L) = \frac{d^2z}{dx^2}(-L) = \frac{d^2z}{dx^2}(L) = 0 \quad (\text{Free} - \text{Free Beam}) \quad (5.3)$$

The solutions to these systems are the following:

$$z(x) = \frac{i_e B L^4}{24EI} \left(\left(\frac{x}{L} \right)^4 - 2 \left(\frac{x}{L} \right)^2 + 1 \right) \quad (C - C \text{ beam}) \quad (5.4)$$

$$z(x) = \frac{i_e B L^4}{24EI} \left(\left(\frac{x}{L} \right)^4 - 6 \left(\frac{x}{L} \right)^2 + 5 \right) \quad (F - F \text{ beam}) \quad (5.5)$$

Ex: for $i_e = 1 \text{ mA}$, $B = 1 \text{ T}$, $E = 70 \text{ GPa}$, $w = 5 \text{ }\mu\text{m}$, $t = 1 \text{ }\mu\text{m}$, $2L = 300 \text{ }\mu\text{m}$, we get a mid-point deflection $w_0 = \frac{5i_e B L^4}{24EI} = 3.6 \text{ }\mu\text{m}$. If we account for a resistivity of Aluminum of $\rho = 2.8e^{-8} \text{ }\Omega.m$, we get a dc power dissipated for moving the beam $P = \frac{2\rho L}{wt} i_e^2 = 1.68 \text{ }\mu\text{W}$.

5.2.2 Uniformly Loaded Beam in Contact with a Solid Wall

We consider here the case of a free-free beam (boundary condition (5.3)), and add a constraint given by a rigid wall at distance H from the rest position of the beam (see fig. 5.1). When the contact is made, equation (5.5) has to be modified to account for the constraint. We can distinguish two cases: for a moderate load, the contact is made at only one point; if we continue to increase the load above a critical point, a line contact exist.

- Point contact: for $\frac{24EIH}{5L^4} \leq i_e B \leq \frac{24EIH}{L^4}$

We call R_0 the force exerted by the wall on the beam at the contact point $x = 0$, and M_0 the moment at $x = 0$. We have:

$$EI \frac{d^2z}{dx^2} = \frac{i_e B x^2}{2} - R_0 x - M_0 \quad (5.6)$$

$$z(x) = \frac{i_e B x^4}{24EI} - \frac{R_0 x^3}{6EI} - \frac{M_0 x^2}{2EI} + H \quad (5.7)$$

Solving for the boundary condition at $x = L$, we get:

$$R_0 = \frac{3EI}{L^3} \left(\frac{5i_e B L^4}{24EI} - H \right) > 0 \quad (\text{since } i_e B > \frac{24EIH}{5L^4}) \quad (5.8)$$

$$M_0 = \frac{3EIH}{L^2} - \frac{i_e B L^2}{8} > 0 \quad (\text{since } i_e B < \frac{24EIH}{L^4}) \quad (5.9)$$

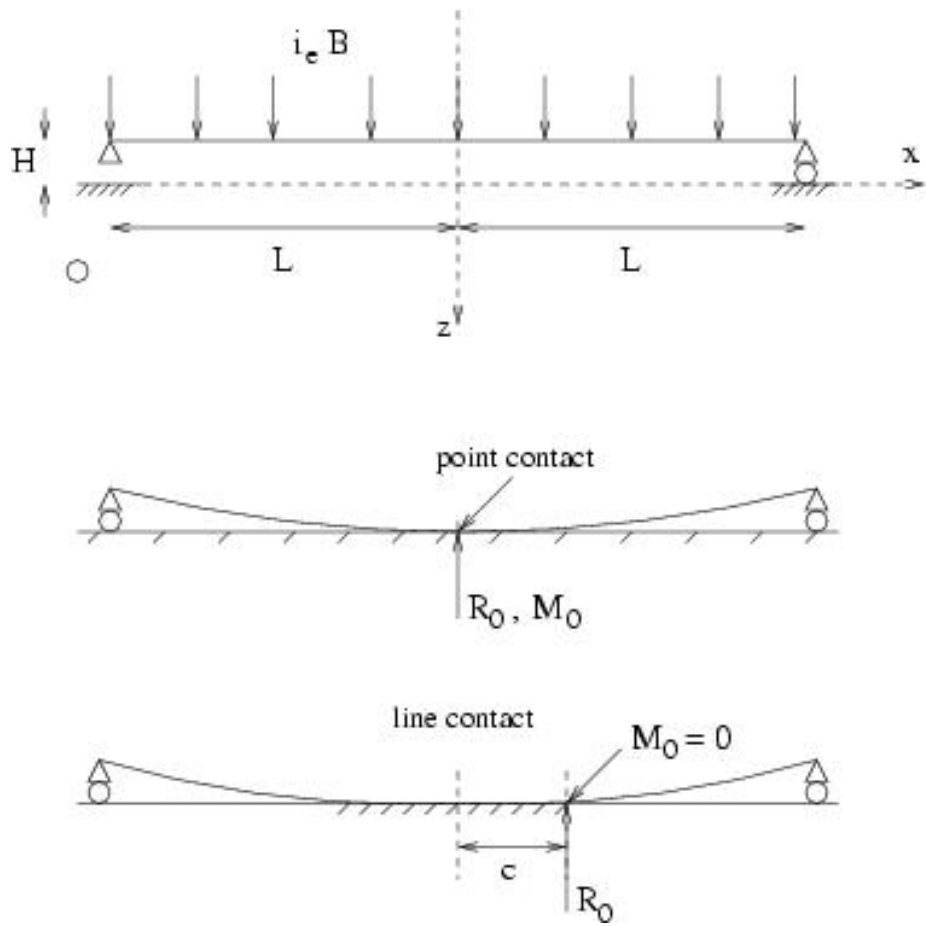


Figure 5.1: Schematic of the beam for the study of the contact with a rigid wall.

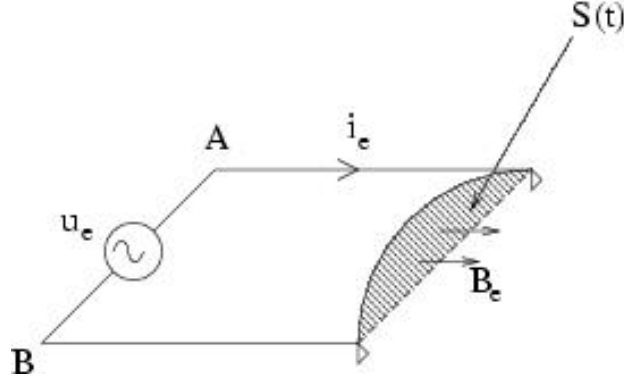


Figure 5.2: Voltage driven circuit with a movable part in a uniform magnetic field.

- Line contact along $-c < x < c$: for $\frac{24EIH}{L^4} < i_e B$
 Here the curvature is 0 at the point where the beam leaves the contact, so there is no moment. We obtain:

$$z(x) = \frac{i_e B(x-c)^4}{24EI} - \frac{R_0(x-c)^3}{6EI} + H \quad (5.10)$$

and solving again for the boundary condition $x = L$:

$$R_0 = \frac{i_e B(L-c)}{2} \quad (5.11)$$

$$c = L - \left(\frac{24EIH}{i_e B}\right)^{\frac{1}{4}} > 0 \text{ (since } i_e B > \frac{24EIH}{L^4} \text{)} \quad (5.12)$$

5.3 Dynamic Analysis

5.3.1 Electromagnetic Damping

In general, the magnetic field created by the current in the beam can easily be neglected compared to the strong external field. In this section, we evaluate the impact of the magnetic damping, due to the fact that we have a movable conductor in a magnetic field. In general, we will neglect this effect, but it is worth mentioning since it is the same phenomena that guided our discussion on filtering applications in 3.4.

The circuit configuration is shown on figure 5.2. A voltage source drives the circuit, which has a movable part. This part is placed in a uniform transverse magnetic field and is allowed to move vertically, therefore when a current flows in the circuit, a displacement occurs under the action of the Lorentz forces.

The electromagnetic damping occurring in this experiment is related to the fact that considering the magnetic system equations, the electric field \mathbf{E}' in

a coordinate system with a speed \mathbf{v} with respect to the reference coordinate system, where the fields are \mathbf{E} and \mathbf{B} , is given by:

$$\mathbf{E}' = \mathbf{E} + \mathbf{v} \wedge \mathbf{B} \quad (5.13)$$

And Ohm's law $\mathbf{J}' = \sigma \mathbf{E}'$ is valid in the coordinate system moving with the media.

If we consider $C(t)$ as the contour of the circuit deforming with time and $S(t)$ a corresponding surface oriented as usual, we can write the integral form of Maxwell-Faraday's equation:

$$\oint_C \mathbf{E}' \cdot d\mathbf{l} = -\frac{d}{dt} \iint_S \mathbf{B}_e \cdot \mathbf{n} dS \quad (5.14)$$

Now the source is in a region where there is no change of magnetic field with time, thus we can decompose the left hand side:

$$\begin{aligned} V_A - V_B &= -\int_B^A \mathbf{E}' \cdot d\mathbf{l} = u_e \\ u_e - \int_A^B \mathbf{E}' \cdot d\mathbf{l} &= \frac{d}{dt} \iint_S \mathbf{B}_e \cdot \mathbf{n} dS \\ u_e - \frac{1}{\sigma} \int_A^B \mathbf{J}' \cdot d\mathbf{l} &= \frac{d}{dt} \iint_S \mathbf{B}_e \cdot \mathbf{n} dS \\ u_e - Ri_e &= \frac{d}{dt} \iint_S \mathbf{B}_e \cdot \mathbf{n} dS \end{aligned}$$

where R represents the total resistance of the circuit.

Thus we see that when we drive the circuit with a voltage source, the current is given by:

$$i_e = \frac{u_e}{R} - \frac{1}{R} \frac{d}{dt} \iint_S \mathbf{B}_e \cdot \mathbf{n} dS \quad (5.15)$$

And in our case where the deflection is in the vertical plane and the magnetic field uniform and parallel to the normal vector, we get:

$$i_e = \frac{u_e}{R} - \frac{B_e}{R} \frac{dS}{dt}$$

where $S(t)$ can be reduced to the area limited by the beam's position in the reference and current configurations.

We see how this expression will induce a damping force on the beam: when the area increases under the action of the Lorentz forces, the current decreases and therefore the forces decrease. In the following here, we will consider that we can control the current inside the circuit, and therefore we do not consider this magnetic damping.

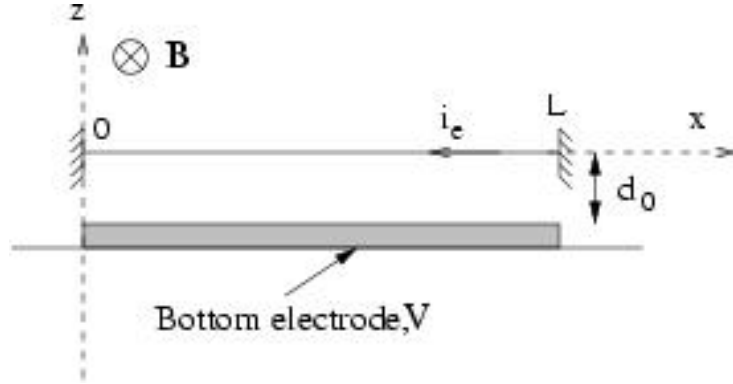


Figure 5.3: Setup for the determination of the switching time.

5.3.2 Switching Speed. Transient Response of the Beam Subject to a Dual Magnetic and Electrostatic Actuation

The goal of this section is to evaluate the switching time for a simple beam subject to a Lorentz and an electrostatic force. The voltage applied is too small to move the beam from the up position, but it will be sufficient to maintain the beam in the down position. The beam is doubly clamped and its dimensions are $L = 300\mu\text{m}$, $w = 5\mu\text{m}$, $t = 1\mu\text{m}$ for the numerical simulations. It is placed in a magnetic field of 1 T . The setup is shown on fig. 5.3.

We implement a Galerkin method similar to the one employed in [38] to solve the PDE describing the evolution of the beam. No damping is taken into account in the simulations, but in any case it should be small with the small width considered for the beam. We do not take any prestress into account either. The switching time is also compared to finite elements simulations carried out with the commercial software Ansys.

Note that for a practical system, this beam would probably be of little interest, since the area is quite small to use as a DC switch or a capacitor, and the spring constant considered in the numerical simulations is too low to insure a good reliability and avoid stiction. But the method is developed to demonstrate the interest of magnetic actuation when the electrodes are far from each other, and we could imagine a release facilitated by pulsed Lorentz forces, as already mentioned [31].

The general equation governing the dynamics of the beam is:

$$\rho_0 A \frac{\partial^2 z}{\partial t^2} + EI \frac{\partial^4 z}{\partial x^4} = -i_e B - \frac{\epsilon_0 w V^2}{(d_0 + z)^2} \quad (5.16)$$

where $A = wt$, ρ_0 is the density, E is the Young's modulus of the beam, I is the modulus of inertia, z is the vertical displacement at position x (see fig. 5.3).

We look for solutions of the form:

$$z(x, t) = \sum_{n=1}^{\infty} \eta_n(t) z_n(x) \quad (5.17)$$

with $z_i(x)$ eigenmodes of the free vibration problem.

Looking for solutions of the form $z(x, t) = f(x) \cos(\omega t)$ for the free vibrations leads to the equation determining $z_n(x)$:

$$\frac{d^4 z_n}{dx^4} - \frac{\omega_n^2 \rho_0 A}{EI} z_n = 0 \quad (5.18)$$

The (normalized) solution for z_n is then:

$$z_n(x) = \gamma_n \left[\frac{\cos(\mu_n) - \cosh(\mu_n)}{-\sin(\mu_n) + \sinh(\mu_n)} \left[-\sin(\mu_n \frac{x}{L}) + \sinh(\mu_n \frac{x}{L}) \right] - \cos(\mu_n \frac{x}{L}) + \cosh(\mu_n \frac{x}{L}) \right] \quad (5.19)$$

with

$$\gamma_n^2 = \frac{1}{\rho_0 A L \int_0^1 \left[\frac{\cos(\mu_n) - \cosh(\mu_n)}{-\sin(\mu_n) + \sinh(\mu_n)} \left[-\sin(\mu_n y) + \sinh(\mu_n y) \right] - \cos(\mu_n y) + \cosh(\mu_n y) \right]^2 dy} \quad (5.20)$$

and the modal frequencies are determined as follows:

$$\cos(\mu_n) \cosh(\mu_n) = 1, \quad \omega_n^2 = \mu_n^4 \frac{EI}{\rho_0 A L^4} \quad (5.21)$$

we have

$$\begin{aligned} \mu_1 &\approx 4.730 \\ \mu_2 &\approx 7.853 \\ \mu_3 &\approx 10.996 \\ \mu_n &\approx (2n + 1) \frac{\pi}{2} \end{aligned} \quad (5.22)$$

Note that with this normalization, we have the following relationships [39]:

$$\rho_0 A \int_0^L z_n(x) z_m(x) dx = \delta_{n,m} \quad (5.23)$$

$$\int_0^L \frac{d^2 z_n}{dx^2}(x) \frac{d^2 z_m}{dx^2}(x) dx = \frac{\omega_n^2}{EI} \delta_{n,m} \quad (5.24)$$

Now we first use (5.17) into (5.16):

$$\rho_0 A \sum_{i=1}^{\infty} \ddot{\eta}_i(t) z_i(x) + EI \sum_{i=1}^{\infty} \eta_i(t) \frac{d^4 z_i}{dx^4}(x) = i_e B - \frac{\epsilon_0 w V^2}{(d_0 + z(x, t))^2}$$

Next we multiply by $z_j(x)$ and integrate between $x = 0$ and $x = L$:

$$\begin{aligned} \sum_{i=1}^{\infty} \ddot{\eta}_i(t) \rho_0 A \int_0^L z_i(x) z_j(x) dx + \sum_{i=1}^{\infty} \eta_i(t) EI \int_0^L \frac{d^4 z_i}{dx^4}(x) z_j(x) dx \\ = \int_0^L i_e B z_j(x) dx - \int_0^L \frac{\epsilon_0 w V^2}{(d_0 + z(x, t))^2} z_j(x) dx \end{aligned}$$

that is, after 2 integrations by parts and using (5.23) and (5.24):

$$\ddot{\eta}_j(t) + \omega_j^2 \eta_j(t) = \int_0^L i_e B z_j(x) dx - \int_0^L \frac{\epsilon_0 w V^2}{(d_0 + z(x, t))^2} z_j(x) dx, \quad j = 1 \dots n \quad (5.25)$$

The second term on the right hand side, due to the electrostatic force, complicates the resolution of the system since it induces a coupling between all the equations through the term $z(x, t)$ in the denominator, which includes all modes. The difficulty is also linked to the dependance on time present in this term. Because of this, we developed a finite different scheme to solve the system numerically. Special care is needed when z approaches $-d_0$ since then this term blows up. To avoid this problem, we stopped the computation when the beam comes close enough to the electrode, selecting the convergence criteria manually.

The numerical implementation can be summarized in the following steps:

- compute μ_n and ω_n with (5.21).
- compute γ_n with (5.20).
- compute the RHS terms of (5.16) at time t . Use the initial condition to start.
- compute all η_j at time $t + \Delta t$ using (5.16), with a forward-backward difference scheme.
- we have all the elements to compute the terms at time $t + \Delta t$.

Fig. 5.4 shows the shape of the beam during the response to a step load of magnetic and electrostatic force, as well as the position of the midpoint with time and thus the switching time. We see that with the values considered, we obtain a switching time of around $7 \mu s$.

To verify the scheme, it is possible to compare the results given when we set $V = 0$ with the theoretical formula. Indeed, when there is no nonlinear term due to the electrostatic force, the differential equations are decoupled and the general solution for η_j becomes:

$$\text{for } V = 0: \quad \eta_j(t) = \frac{(i_e B \int_0^L z_j(x) dx)}{\omega_j^2} (1 - \cos(\omega_j t))$$

The numerical scheme is shown in this case to provide results very close to the theoretical values.

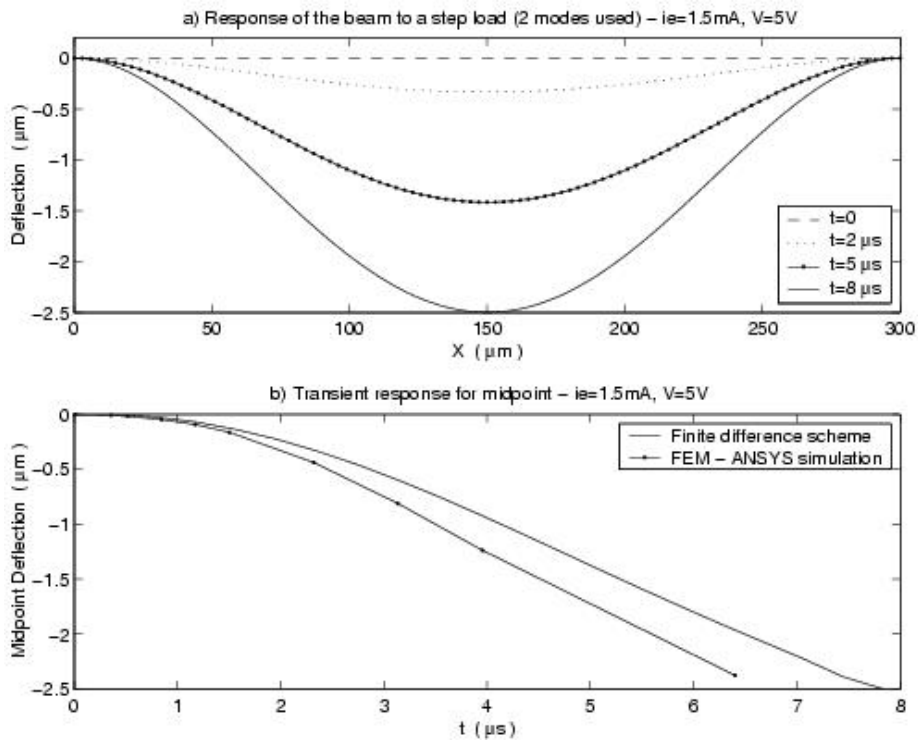


Figure 5.4: Transient response of the beam to a load of magnetic and electrostatic force. The gap between the electrodes is $2.5\ \mu\text{m}$. a) Shape of the beam at different instants. b) Position of the midpoint until the first contact.

5.3.3 Finite Elements Dynamics Simulation

Finite elements simulations have been carried out with ANSYS for the dual magnetic and electrostatic actuation, and results for the switching time have been compared to the results obtained in the previous section. The simulation were done using the transducer element TRANS126 for the electro-mechanical coupling. The elements were generated along the beam using the macro EMT-GEN. Due to the simplicity of the geometry and the small deformations, we did not have to use a more involved technique such as TRANS109. A uniform load was added to account for the magnetic force.

Part III

Stability Study

Chapter 6

Problems of Stability for a Beam in a Non Uniform Magnetic Field

6.1 Introduction

The goal of this document is to present the mechanical stability properties of a beam conducting a current in a non-uniform magnetic field. This is motivated by trying to understand the type of unstability which can occur in the case of the capacitive switch with magnetic actuation. In order to derive an analytical model, some hypothesis have to be made, which changes the configuration of interest. However, the result should provide some information on the mechanical behavior of the original beam, and a way to evaluate the validity of future numerical calculations.

Thus we consider a beam attached at its extremities (the boundary conditions can be simply supported or clamped) and suspended in a magnetic field created by two infinitely permeable plates with a difference of magnetic total potential ψ_0 . In the reference configuration, this beam is exactly on the middle line between the two plates (figure 6.1). When a current is sent through the beam, it moves under the action of the Lorentz forces $\mathbf{F} = \mathbf{i} \wedge \mathbf{B}$. Thus in this configuration, we exaggerate the non uniformity of the magnetic field by replacing the thick magnets by infinitely thin plates (the plates are infinite in the x -direction (see 6.1)).

This configuration seems to be unstable: we see that in the ideal configuration, the deflection of the beam happens in the middle plane and the magnetic forces are purely vertical, but if a lateral deflection of the beam occurs, a lateral component in the magnetic forces appears, which tends to accentuate the deflection. Therefore, we should find a critical value for the magnetic forces, at which the stiffness of the beam is not sufficient to compensate these lateral

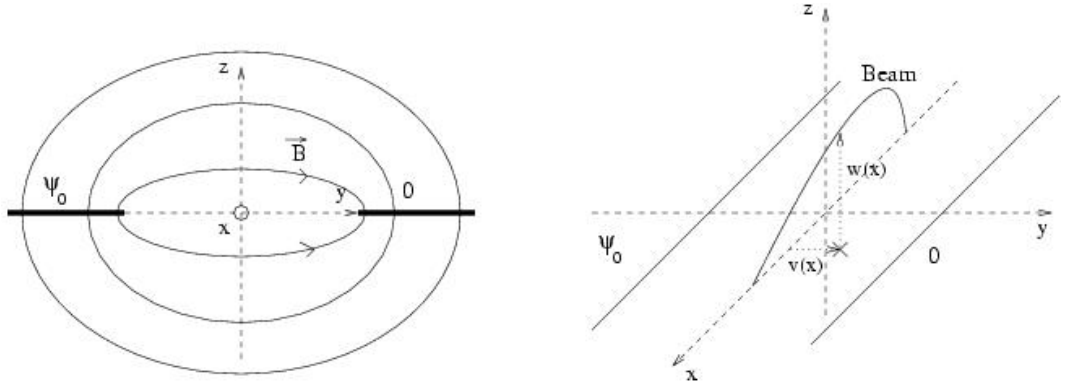


Figure 6.1: Configuration of the beam between two infinitely permeable infinite plates.

magnetic forces, and thus the vertical equilibrium becomes unstable.

6.2 Potential Energy Associated with the Lorentz Forces

6.2.1 Work Done by the Lorentz Forces for a Portion of Lineic Circuit in \mathbf{B}_{ext} .

For a portion δl of the circuit, with a current i , subject to a small displacement $\delta s = v dt$:

$$\begin{aligned}
 \delta^2 W_e &= i (\delta \mathbf{l} \wedge \mathbf{B}_{ext}) \cdot \delta \mathbf{s} \\
 &= i (\delta \mathbf{s} \wedge \delta \mathbf{l}) \cdot \mathbf{B}_{ext} \\
 &= i \delta^2 \Sigma \cdot \mathbf{B}_{ext} \\
 &= i \delta^2 \phi_c^e
 \end{aligned} \tag{6.1}$$

where $\delta^2 \phi_c^e$ is the flux cut by the infinitely small portion $\delta \mathbf{l}$ of the circuit during the infinitely small displacement $\delta \mathbf{s}$. This can be integrated along the circuit or a part of the circuit:

$$\delta W_e = i \int_{circuit} (\delta \mathbf{s} \wedge \delta \mathbf{l}) \cdot \mathbf{B}_{ext} = i \delta \phi_c^e$$

6.2.2 Maxwell's Theorem

For an infinitely small deformation or a displacement of the circuit, if \mathbf{B}_{ext} is independent of time, and $\Phi_e(t)$ is the flux of \mathbf{B}_{ext} in the circuit ($\Phi_e(t) =$

$\iint_{S_t} \mathbf{B}_{ext} \cdot \mathbf{n} \delta S = \oint_{C_t} \mathbf{A}_{ext} \cdot \delta \mathbf{l}$, with \mathbf{A} being the magnetic potential vector):

$$\begin{aligned} \delta \phi_c^e &= d\Phi_e \\ \delta W_e &= i d\Phi_e \end{aligned} \quad (6.2)$$

The proof is easy and given in annexe A.

6.2.3 Potential Energy When the Current is Constant

Then with $i(t) = I_e$ and \mathbf{B}_{ext} independant of time:

$$\delta W_e = I_e d\Phi_e = d(I_e \Phi_e)$$

And thus a potential energy is associated to the Lorentz forces:

$$E_{pe_{Lorentz}} = -I_e \Phi_e(\text{position and shape of the circuit}) \quad (6.3)$$

Note that a consequence of this is that when only the Lorentz forces work, they tend to maximize the flux in the circuit (minimize E_p).

6.3 Calculation of the Magnetic Flux

In order to set up the energy of the problem, we see that we need to find an expression for the flux of the magnetic field intensity through the circuit. In this paragraph we give the expression of the integrated flux in 2D between any point on the line joining the plates ($z = x = 0$) and any point of the plane (yOz) (see fig. 6.1).

A powerful method is two use a conformal transformation to relate the field of interest here to the simple field of a line current located at the origin ([40]). The map transforming the upper half t -plane into the exterior of the plates in the considered plane (yOz) called Z -plane ($Z = y + jz$) is found by solving the following Schwarz-Christoffel equation:

$$\frac{dZ}{dt} = S \left(1 - \frac{1}{t^2}\right)$$

where S depends on the dimensions of the configuration. If we call $2d$ the distance between the plates therefore the final map is

$$Z = \frac{d}{2} \left(t + \frac{1}{t}\right) \quad (6.4)$$

Note that this map transforms the real axis of the t -plane into the plates in the Z -plane.

Consider now in the t -plane the field due to two semi-infinite equipotential planes, one lying between 0 and ∞ , the other between 0 and $-\infty$, with a difference of potential ψ_0 maintained between the two halves of the real axis,

then the field in the positive half plane is described by the complex potential function:

$$\phi + j\psi = \frac{\psi_0}{\pi} \log t \quad (6.5)$$

This is the same field as the field created by a current line at the origin with a current equal to ψ_0 through it (the line creates the potential difference between the two halves of the real axis). The expression for the complex potential of a current line is explained in annexe B. We simply recall that in these equations, ψ is the magnetic potential ($\mathbf{H} = -\nabla\psi$ for regions without currents and in the exterior ψ obeys Laplace's equation), and $\phi = \text{constant}$ defines a flux line, that is $\phi = \phi_0$ and $\phi = \phi_0 + n$ have n units of flux passing between them.

Eliminating t between (6.4) and (6.5) gives us the expression of the relation between the position in the actual Z -plane and the complex potential:

$$Z = y + jz = d \cosh\left(\frac{\pi}{\psi_0}(\phi + j\psi)\right) \quad (6.6)$$

This expression has to be inverted because we need the expression of the flux function at each point (y, z) . The inversion of (6.6) leads to the following flux function (valid outside the plates):

$$\phi(y, z) = \frac{\psi_0}{2\pi} \operatorname{arccosh}(f(y, z)) \times \operatorname{sign}(y) \quad (6.7)$$

$$f(y, z) = \frac{y^2}{d^2} + \frac{z^2}{d^2} + \sqrt{\frac{z^4}{d^4} + \frac{2z^2}{d^2} + \frac{2y^2z^2}{d^4} + \left(1 - \frac{y^2}{d^2}\right)^2} \quad (6.8)$$

Note here that the line $z = 0, |y| \leq d$ corresponds to the flux line $\phi = 0$ therefore $\phi(y, z)$ directly gives the flux passing between the point (y, z) and any point of the line between joining the plates, in particular it gives the flux passing between (y, z) and the origin.

6.4 Mechanical Problem Formulation

We now have all the information needed to set up the energy of the problem. In this study, we consider small deformations of the beam, and therefore it leads to the following simplifications:

- The internal energy can be written:

$$E_{int} = \frac{1}{2} \int_0^L (EI_{yy}w_{,xx}^2 + EI_{zz}v_{,xx}^2) dx \quad (6.9)$$

- The energy associated to the Lorentz forces is the difference between the potential energy in the reference and the current configuration and can be written $E_{em} = -I_e \Delta \Phi_e$, with the usual orientation of the normal vector

compatible with the direction of the current for a surface enclosed by a lineic circuit. If we consider that the only part of the circuit moving between the two configurations is the beam, then the term $\Delta\Phi_e$ is the flux passing through the area enclosed by the curve describing the beam in the two configurations. Because of the small deformations hypothesis, the length L for the integration along direction (Ox) in both configurations is the same, without any corrective term (we neglect the cosine of the angle of the tangent line to the beam with the (Ox) direction). The original configuration corresponds to the axis (Ox) and $\phi(y, z) = 0$. To compute the total flux we integrate the infinitesimal flux at position x given by $\phi(v(x), w(x))$, where v and w are the horizontal and vertical displacements of the beam in the final configuration (see fig. 6.1). Thus the magnetic energy is given by:

$$E_{em} = -I_e \int_0^L \phi(v(x), w(x)) dx \quad (6.10)$$

where ϕ is the expression given in (6.7).

- In the following, we will often make the approximation $\frac{w}{d} \ll 1$ in order to obtain a tractable solution.

Adding (6.9), (6.10) and gives the expression of the energy for the problem:

$$E(\mathbf{u}) = E(v, w) = \frac{1}{2} \int_0^L (EI_{yy} w_{,xx}^2 + EI_{zz} v_{,xx}^2) dx - I_e \int_0^L \phi(v(x), w(x)) dx$$

6.5 Equilibrium and Stability

6.5.1 Equilibrium Equations. Fundamental Solution

Evaluating the stability of the system can essentially be done in a way similar to [41]. The first derivative of the energy given in (6.11) provides the equilibrium equations.

$$\begin{aligned} E_{,\mathbf{u}}(\mathbf{u})[\delta\mathbf{u}] &= \int_0^L (EI_{yy} w_{,xxxx} \delta w + EI_{zz} v_{,xxxx} \delta v \\ &\quad - I_e \frac{\partial\phi}{\partial v}(v(x), w(x)) \delta v - I_e \frac{\partial\phi}{\partial w}(v(x), w(x)) \delta w) dx \\ &+ [w_{,xx} \delta w_{,x}]_0^L - [w_{,xxx} \delta w]_0^L + [v_{,xx} \delta v_{,x}]_0^L - [v_{,xxx} \delta v]_0^L \end{aligned} \quad (6.11)$$

And thus here are the equilibrium equations:

$$\delta v \text{ terms} : EI_{zz}v_{,xxxx} - I_e \frac{\partial \phi}{\partial v} = 0 \quad (6.12)$$

$$\delta w \text{ terms} : EI_{yy}w_{,xxxx} - I_e \frac{\partial \phi}{\partial w} = 0 \quad (6.13)$$

$$B.C. : v(0) = v(L) = w(0) = w(L) = 0 \quad (6.14)$$

$$v_{,xx}(0) = v_{,xx}(L) = w_{,xx}(0) = w_{,xx}(L) = 0 \text{ (s.s.)} \quad (6.15)$$

$$v_{,x}(0) = v_{,x}(L) = w_{,x}(0) = w_{,x}(L) = 0 \text{ (clamped)} \quad (6.16)$$

We provide the expression of $\frac{\partial \phi}{\partial v}$ and $\frac{\partial \phi}{\partial w}$ in annexe C. We verify that $\frac{\partial \phi}{\partial v}(0, w) = 0$, and consider the following approximation of the fundamental solution ($v = 0, w = \hat{w}$) where:

$$\hat{w} = \frac{I_e B_0}{24EI_{yy}} x(x-L)(x^2 - Lx - L^2) \text{ (s.s. beam)} \quad (6.17)$$

$$\hat{w} = \frac{I_e B_0}{24EI_{yy}} x^2(x-L)^2 \text{ (clamped beam)} \quad (6.18)$$

$$(6.19)$$

This equation for ($v = 0, w = \hat{w}$) corresponds to the approximation $\frac{w}{d} \ll 1$ where (6.13) becomes for $v = 0$:

$$EI_{yy}\hat{w}_{,xxxx} = I_e B_0 \frac{1}{\sqrt{1 + \frac{\hat{w}^2}{d^2}}} \approx I_e B_0, \quad B_0 = \frac{\psi_0}{\pi d} \quad (6.20)$$

B_0 is the value of the magnetic field density at the origin. In the following, we take $I_e > 0$ and thus the fundamental solution corresponds to $\hat{w} > 0$.

6.5.2 Stability of the Equilibrium

The second derivative can be written:

$$\begin{aligned} E_{,uu}(\hat{\mathbf{u}})[\tilde{\mathbf{u}}, \delta \mathbf{u}] &= \int_0^L (EI_{yy}\tilde{w}_{,xxxx} \delta w + EI_{zz}\tilde{v}_{,xxxx} \delta v \\ &- I_e \frac{\partial^2 \phi}{\partial v^2}(\hat{\mathbf{u}}) \tilde{v} \delta v - I_e \frac{\partial^2 \phi}{\partial w^2}(\hat{\mathbf{u}}) \tilde{w} \delta w - I_e \frac{\partial^2 \phi}{\partial v \partial w}(\hat{\mathbf{u}}) [\tilde{w} \delta v + \tilde{v} \delta w]) dx \\ &+ [\tilde{w}_{,xx} \delta w_{,x}]_0^L - [\tilde{w}_{,xxx} \delta w]_0^L + [\tilde{v}_{,xx} \delta v_{,x}]_0^L - [\tilde{v}_{,xxx} \delta v]_0^L \end{aligned} \quad (6.21)$$

If we look at the critical point where the definite positiveness might be lost, we get the following equations for \tilde{u} :

$$EI_{zz}\tilde{v}_{,xxxx} - I_e \frac{\partial^2 \phi}{\partial v^2}(\hat{\mathbf{u}}) \tilde{v} - I_e \frac{\partial^2 \phi}{\partial v \partial w}(\hat{\mathbf{u}}) \tilde{w} = 0 \quad (6.22)$$

$$EI_{yy}\tilde{w}_{,xxxx} - I_e \frac{\partial^2 \phi}{\partial w^2}(\hat{\mathbf{u}}) \tilde{w} - I_e \frac{\partial^2 \phi}{\partial v \partial w}(\hat{\mathbf{u}}) \tilde{v} = 0 \quad (6.23)$$

$$\tilde{v}(0) = \tilde{v}(L) = \tilde{w}(0) = \tilde{w}(L) = 0 \quad (6.24)$$

$$\text{and } \tilde{v}_{,xx}(0) = \tilde{v}_{,xx}(L) = \tilde{w}_{,xx}(0) = \tilde{w}_{,xx}(L) = 0 \text{ (s.s.)} \quad (6.25)$$

$$\text{or } \tilde{v}_{,x}(0) = \tilde{v}_{,x}(L) = \tilde{w}_{,x}(0) = \tilde{w}_{,x}(L) = 0 \text{ (clamped)} \quad (6.26)$$

It turns out that the expression of the terms involving the second derivative of the magnetic flux along the fundamental solution $\hat{\mathbf{u}} = (v = 0, w = \hat{w})$ simplify and give the following system for (6.22) and (6.23) (I_e and \hat{w} positive):

$$EI_{zz}\tilde{v}_{,xxxx} - I_e \frac{B_0}{d} \frac{\frac{\hat{w}}{d}}{(1 + (\frac{w}{d})^2)^{\frac{3}{2}}} \tilde{v} = 0 \quad (6.27)$$

$$EI_{zz}\tilde{w}_{,xxxx} + I_e \frac{B_0}{d} \frac{\frac{\hat{w}}{d}}{(1 + (\frac{w}{d})^2)^{\frac{3}{2}}} \tilde{w} = 0 \quad (6.28)$$

That is, in the limit where $\frac{\hat{w}}{d} \ll 1$, and for the simply supported beam:

$$EI_{zz}\tilde{v}_{,xxxx} - (I_e B_0)^2 \frac{x(x-L)(x^2 - Lx - L^2)}{24EI_{yy}d^2} \tilde{v} = 0 \quad (6.29)$$

$$EI_{yy}\tilde{w}_{,xxxx} + (I_e B_0)^2 \frac{x(x-L)(x^2 - Lx - L^2)}{24EI_{yy}d^2} \tilde{w} = 0 \quad (6.30)$$

$$\tilde{v}(0) = \tilde{v}(L) = \tilde{w}(0) = \tilde{w}(L) = 0 \quad (6.31)$$

$$\tilde{v}_{,xx}(0) = \tilde{v}_{,xx}(L) = \tilde{w}_{,xx}(0) = \tilde{w}_{,xx}(L) = 0 \quad (6.32)$$

Given the boundary conditions already established, we want to know for which values of $I_e B_0$ we can find a non trivial solution $\tilde{\mathbf{u}}$. We do not try to solve directly the previous equations, but we will use variational methods here.

Solving the differential equation (6.30) with the boundary conditions for w is equivalent to the following minimization problem:

$$\tilde{w} = \arg \min_{w, w(0)=w(L)=0} \left[\int_0^L \left(EI_{yy} w_{,xx}^2 + (I_e B_0)^2 \frac{x^2(x-L)^2}{24EI_{yy}d^2} w^2 \right) dx \right] \quad (6.33)$$

We can prove by a convexity argument that this problem has a unique minimum, which is then $\tilde{w}(x) = 0$. Because of the negative sign in equation (6.29), this argument does not apply any more in the v-equation (convexity lost) and we can try to find an other minimum to the variational problem corresponding to (6.29). Therefore we see that there is a possibility of unstability only in the v-direction, the w-direction is stable as expected.

Table 6.1: Numerical factor in the upper bound of the critical load $(I_e B_0)_c$, with Fourier expansions.

Nb.	Terms	s.s. beam	clamped beam
1		8786.8	232860
5		8782.6	227410
10		8782.6	227271
30		8782.6	227248
50		8782.6	227247

6.5.3 Critical Loads for the Instability in the v-direction

Simply Supported Beam Moving Up

It is proved in annexe D that the critical load $I_e B_0$ below which a non trivial solution \tilde{v} exists is given by (for the s.s. beam):

$$(I_e B_0)_{c,free}^2 = \frac{24E^2 d^2 I_{yy} I_{zz}}{L^8} \min_{v, v(0)=v(1)=0} \frac{\int_0^1 v_{,yy}^2 dy}{\int_0^1 y(y-1)(y^2-y-1)v^2 dy} \quad (6.34)$$

For the clamped beam, we will need to add to the space of test functions the essential boundary conditions $v_{,x}(0) = v_{,x}(1) = 0$.

A first approximation of this load for the s.s. beam is given by taking a test function $v = A_1 \sin(\pi x)$. Then we obtain the following expression:

$$(I_e B_0)_{c,free}^2 \leq \frac{24E^2 d^2 I_{yy} I_{zz}}{L^8} \frac{10\pi^8}{2\pi^4 + 5\pi^2 + 15} \approx 8787 \frac{E^2 d^2 I_{yy} I_{zz}}{L^8} N.m^{-1}$$

Using a more complete Fourier expansion of $v = \sum_{i=1}^n A_n \sin(n\pi x)$ leads to slightly lower results for the numerical factor (see table 6.1) but the convergence is very quick.

Clamped Beam Moving Up

For the clamped beam, the critical load is given by:

$$(I_e B_0)_{c,clamped}^2 = \frac{24E^2 d^2 I_{yy} I_{zz}}{L^8} \min_{\substack{v, v(0)=v(1)=0 \\ v_{,x}(0)=v_{,x}(1)=0}} \frac{\int_0^1 v_{,yy}^2 dy}{\int_0^1 y^2(y-1)^2 v^2 dy} \quad (6.35)$$

Here we first try a test function $v(x) = A_1(1 - \cos(2\pi x))$ and we get:

$$(I_e B_0)_{c,clamped}^2 \leq \frac{24E^2 d^2 I_{yy} I_{zz}}{L^8} \frac{2560\pi^8}{16\pi^4 + 945} \approx 232860 \frac{E^2 d^2 I_{yy} I_{zz}}{L^8} N.m^{-1}$$

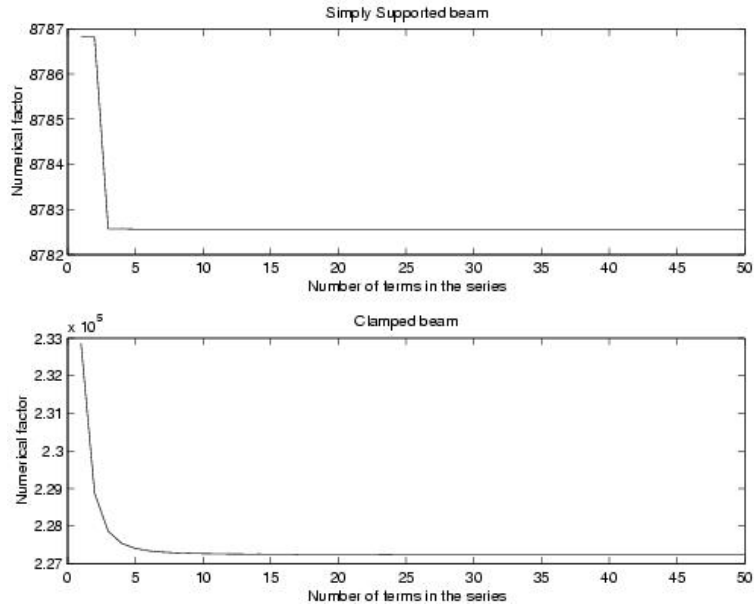


Figure 6.2: Convergence of the numerical prefactor, for the simply supported and clamped beams.

6.6 Numerical Results

As an example we compute the upper limits obtained for the load in the case of the beam moving up. The beam had a thickness of $1 \mu m$, a width of $5 \mu m$, a length of $300 \mu m$ and is made out of aluminum ($E = 70 GPa$). We suppose $d = 30 \mu m$.

We obtain then, for the simply supported beam:

$$(I_e B_0)_{c,free} \leq 2.56 \times 10^{-3} A.T$$

This shows that the system is quite unstable in the range of values considered so far. But this is due mostly to a large exaggeration of the geometric nonlinearities of the field created here by thin plates. In the case of a doubly clamped beam, the structure is of course more stable:

$$(I_e B_0)_{c,clamped} \leq 66.3 \times 10^{-3} A.T$$

Conclusion

Part IV
Appendix

Appendix A

Demonstration of the Maxwell's Theorem

For an infinitely small increment of time, and a displacement or deformation of a lineic circuit in a uniform and permanent magnetic field (see fig. A.1):

$(S_t) \cup (\Sigma) \cup (S_{t+dt})$ is a closed surface therefore $\iint \mathbf{B}_e \cdot \mathbf{n}_{ext} \delta S = 0$, which can be decomposed (the normal vector \mathbf{n} is oriented relatively to the direction of the current i in the circuit):

$$\begin{aligned} \iint_{S_{t+dt}} \mathbf{B}_e \cdot \mathbf{n} \delta S - \delta\phi_c^e - \iint_{S_t} \mathbf{B}_e \cdot \mathbf{n} \delta S &= 0 \\ \Phi_e(t+dt) - \Phi_e(t) &= \delta\phi_c^e \text{ if } \mathbf{B}_e \text{ permanent} \\ d\Phi_e &= \delta\phi_c^e \end{aligned}$$

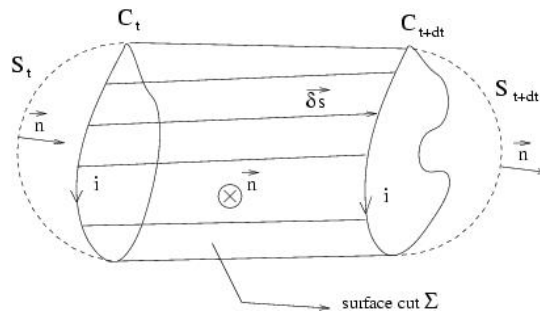


Figure A.1: Infinitely small Displacement/Deformation of a lineic circuit in a uniform and permanent magnetic field.

Appendix B

Complex Potential Due to a Line Current

We know that the magnetic field created by a line current is:

$$B = \frac{\mu_0 \mu i}{2\pi r} \quad (\text{B.1})$$

with i the current in the line and r the distance to the line.

The flux passing between two points at radii r_1 and r_2 is

$$\int_{r_1}^{r_2} \frac{\mu_0 \mu i}{2\pi r} dr = \frac{\mu_0 \mu i}{2\pi} [\log r]_{r_1}^{r_2}$$

the flux function is proportional to this and usually expressed in a form independent of $\mu_0 \mu i$ as:

$$\phi = \frac{1}{2\pi} \log r \quad (\text{B.2})$$

The potential function ψ (total scalar potential) and the flux function can be derived from each other (see [40]) and are related by the Cauchy-Riemann equations. In polar coordinates, we get:

$$\psi = \int r \frac{\partial \phi}{\partial r} d\theta = \frac{1}{2\pi} \theta + f(r)$$

From symmetry, ψ is a function of θ only and $f(r)$ is equal to an arbitrary constant which can be ignored, so the potential function can be expressed:

$$\psi = \frac{1}{2\pi} \theta \quad (\text{B.3})$$

It is now apparent that (B.2) and (B.3) can be combined to form the complex magnetic potential:

$$w = \phi + j\psi = \frac{1}{2\pi} \log(re^{j\theta}) = \frac{1}{2\pi} \log t \quad (\text{B.4})$$

Appendix C

Expression of the Flux Function and its Derivatives

In the space between the two plates ($-d \leq v \leq d$) in chapter 6, the magnetic flux function is given by:

$$\phi(v, w) = \frac{\psi_0}{2\pi} \operatorname{arccosh}(f(v, w)) \times \operatorname{sign}(v) \quad (\text{C.1})$$

$$f(v, w) = \frac{v^2}{d^2} + \frac{w^2}{d^2} + \sqrt{\frac{w^4}{d^4} + \frac{2w^2}{d^2} + \frac{2v^2w^2}{d^4} + \left(1 - \frac{v^2}{d^2}\right)^2} \quad (\text{C.2})$$

In order to derive the equilibrium and stability equations, we need to derive up to the second derivatives of this flux function. The expressions are given below, and the simplifications arising in the case of the derivation along the fundamental solution are found in the concerned chapter.

First Derivative:

$$\frac{\partial \phi}{\partial w}(v, w) = \frac{\psi_0 v \sqrt{v^2 + w^2 - d^2 + \sqrt{(v^2 + w^2 + d^2)^2 - 4v^2 d^2}}}{\pi \sqrt{v^2 + w^2 + d^2 - 4v^2 d^2} \sqrt{v^2 + w^2 + d^2 + \sqrt{(v^2 + w^2 + d^2)^2 - 4v^2 d^2}}}$$

$$\frac{\partial \phi}{\partial v}(v, w) = \frac{\psi_0 w \sqrt{v^2 + w^2 + d^2 + \sqrt{(v^2 + w^2 + d^2)^2 - 4v^2 d^2}}}{\pi \sqrt{v^2 + w^2 + d^2 - 4v^2 d^2} \sqrt{v^2 + w^2 - d^2 + \sqrt{(v^2 + w^2 + d^2)^2 - 4v^2 d^2}}}$$

Second Derivative:

Given the complexity of the expression for the first partial derivatives, the second partial derivatives were computed using MAPLE and the (long) expressions are not given here. These expressions are greatly simplified when we consider them on the fundamental solution where $v = 0$ and provide the stability equations given in chapter 6.

Appendix D

Variational Problem for the Transverse Direction Stability

D.1 Problem Formulation

In this part, we justify the use of the Rayleigh's quotient in the derivation of the critical load for the stability in chapter 6. Consider the following problem:

$$\text{Find } \min_{v \in V} \frac{\int_0^1 v_{,xx}^2 dx}{\int_0^1 f(x)v^2 dx} \quad (\text{D.1})$$
$$V = \left\{ v \text{ s.t. } \int_0^1 v^2 dx < \infty, \int_0^1 v_{,xx}^2 dx < \infty \right\}, \quad f \text{ continuous } > 0 \text{ on }]0, 1[$$
$$v(0) = v(1) = 0$$

And assume first that we know that a minimizing function \tilde{v} exists, and let us call λ the value of the minimum. Let us prove that \tilde{v} is solution of the

differential equation of interest (6.29).

Let $\epsilon \in \mathbb{R}, v \in V$ then $\tilde{v} + \epsilon v \in V$

We have by definition: $\frac{\int_0^1 (\tilde{v}_{,xx} + \epsilon v_{,xx})^2 dx}{\int_0^1 f(x)(\tilde{v} + \epsilon v)^2 dx} \geq \lambda$

Expanding this formula, using the definition of \tilde{v} , we get:

$$\forall \epsilon, \forall v \in V, \quad \epsilon^2 \int_0^1 (v_{,xx}^2 - \lambda f(x)v^2) dx + 2\epsilon \int_0^1 (\tilde{v}_{,xx} v_{,xx} - \lambda f(x)\tilde{v}v) dx \geq 0$$

Because we allow the sign of ϵ to change, and because the sign of the expression is controlled by the last term for ϵ sufficiently small, we have necessarily:

$$\forall v \in V, \quad \int_0^1 (\tilde{v}_{,xx} v_{,xx} - \lambda f(x)\tilde{v}v) dx = 0$$

After an integration by parts:

$$\forall v \in V, \quad \int_0^1 (\tilde{v}_{,xxxx} - \lambda f(x)\tilde{v})v dx + [\tilde{v}_{,xx} v_{,x}]_0^1 - [\tilde{v}_{,xxx} v]_0^1 = 0$$

The last term disappears by definition of V , and we deduce:

$$\tilde{v}_{,xxxx} - \lambda f(x)\tilde{v} = 0$$

$$\tilde{v}_{,xx}(0) = \tilde{v}_{,xx}(1) = 0 \text{ (and } \tilde{v}(0) = \tilde{v}(1) = 0 \text{ because } \tilde{v} \in V)$$

Note that for the clamped beam, we would need to add the condition $v_{,x}(0) = v_{,x}(1) = 0$ to the definition of V , space of test functions.

Two points remain to finish the demonstration. We want to show that λ is the smallest value for which we have a non trivial solution to the differential equation, and we still need to study the problem of the existence of a minimizing function.

Suppose $\exists \hat{v} \neq 0$ and $\hat{\lambda}$ s.t.

$$\hat{v}_{,xxxx} - \hat{\lambda} f(x)\hat{v} = 0$$

$$\hat{v}_{,xx}(0) = \hat{v}_{,xx}(1) = \hat{v}(0) = \hat{v}(1) = 0$$

$$\text{Thus } \forall v \in V : \int_0^1 \hat{v}_{,xxxx} v dx - \int_0^1 \hat{\lambda} f(x)\hat{v}v dx = 0$$

$$\forall v \in V : \int_0^1 \hat{v}_{,xx} v_{,xx} dx - \int_0^1 \hat{\lambda} f(x)\hat{v}v dx = 0$$

$$\text{Take } v = \hat{v} : \hat{\lambda} = \frac{\int_0^1 \hat{v}_{,xx}^2 dx}{\int_0^1 f(x)\hat{v}^2 dx} \geq \min_{v \in V} \frac{\int_0^1 v_{,xx}^2 dx}{\int_0^1 f(x)v^2 dx}$$

$$\text{That is } \hat{\lambda} \geq \lambda$$

We see that λ is actually the smallest value for which we can have a non trivial solution for our differential equation (and therefore it is called critical load in the mechanical analysis).

Existence of the minimizing function. The denominator functional being positive definite, it induces an inner product and the problem can easily be linked to the following:

$$\text{Find the minimum of } \frac{(Hu, u)}{(u, u)}$$

The positive definite functional $(Hu, u)/(u, u)$ has zero for lower bound and thus has a greatest lower bound λ_1 . Thus there exist a minimizing sequence of functions w_1, \dots, w_n, \dots such that:

$$\frac{(Hw_i, w_i)}{(w_i, w_i)} \rightarrow \lambda_1$$

But we have no garanty a priori that an admissible function u_1 actually realizes this minimum. However, the existence of this minumizing function could be proven using a more precise study of the functional space V , that we do not carry here. ([42]).

D.2 Numerical Determination of the Critical Load

In order to approach the value of the minimum, we use Fourier Series with an increasing number of terms as test functions. An argument of density should prove that when the number of terms of the Fourier series becomes infinite, the Rayleigh's ratio reaches the real minimum. The minimization becomes a minimization on the coefficients of the series, and thus the problem becomes a classical problem of minimizing quadratic functions.

For the case considered so far, let $v = \sum_{k=1}^N A_k \sin(k\pi x)$ (for a clamped beam, we would take $v = \sum_{k=1}^N A_k (1 - \cos(2k\pi x))$). Therefore we get:

$$\begin{aligned} \int_0^1 v_{,xx}^2 dx &= \pi^4 \sum_{k=1}^N \sum_{l=1}^N A_k A_l k^2 l^2 \int_0^1 \sin(k\pi x) \sin(l\pi x) \\ &= \pi^4 \sum_{k=1}^N \sum_{l=1}^N A_k A_l k^2 l^2 C_{k,l} \\ \int_0^1 f(x) v^2 dx &= \sum_{k=1}^N \sum_{l=1}^N A_k A_l \int_0^1 f(x) \sin(k\pi x) \sin(l\pi x) = \sum_{k=1}^N \sum_{l=1}^N A_k A_l D_{k,l} \end{aligned}$$

Let us call $a = [A_1 A_2 \dots A_N]^T$, $C = (C_{k,l})_{1 \leq k, l \leq N}$, $D = (D_{k,l})_{1 \leq k, l \leq N}$. The numerical problem becomes:

$$\text{Find } \min_{a \in \mathbb{R}^N} \frac{a^T \cdot C \cdot a}{a^T \cdot D \cdot a}, C \text{ and } D \text{ positive definite.}$$

The positive definitiveness of C and D comes from the positive definiteness of the original operators on the space function V (recall that $f(x) > 0$ on $]0, 1[$ and to show that the numerator is definite, use the boundary conditions on v). Because D is positive definite, it induces an inner product and this minimization problem can further be related to the classical result:

$$\min_a \frac{a^T \cdot M \cdot a}{a^T \cdot a} = \min\{\lambda, \lambda \text{ eigenvalue of } M\}$$

The numerical calculation is done as follows:

- Compute the square root Δ of D : $D = \Delta^T \cdot \Delta$ (Δ exists because $D > 0$)
- By positive definiteness again, Δ^{-1} exists. Compute it.
-

$$\begin{aligned} \min_a \frac{a^T \cdot C \cdot a}{a^T \cdot D \cdot a} &= \min_a \frac{(\Delta a)^T \cdot (\Delta^{-1})^T \cdot C \cdot \Delta^{-1} \cdot (\Delta a)}{(\Delta a)^T \cdot (\Delta a)} \\ &= \min\{\text{eigenvalues of } ((\Delta^{-1})^T \cdot C \cdot \Delta^{-1})\} \end{aligned}$$

Therefore we see that the computation of the minimum becomes a problem of determining the smallest eigenvalue of a certain matrix. Note also that because of the orthogonality of the sine functions, C is diagonal here. We determined the general form of $C_{k,l}$ and $D_{k,l}$ with MAPLE.

Bibliography

- [1] G.M. Rebeiz and J.B. Muldavin, *RF MEMS Switches and Switch Circuits*, IEEE Microwave Magazine, Vol. 2, Issue 4, Dec. 2001.
- [2] A.-C. Wong, H. Ding and C.T.-C. Nguyen, *Micromechanical Mixer and Filters*, Electron Devices Meeting, 1998. IEDM'98 Technical Digest, International, 6-9 Dec. 1998, p. 471-474.
- [3] *LETI Annual Research Review: RF microswitch*, 06/15/2001, http://www-leti.cea.fr/Commun/Revue_Annuelle/micronanotechs/MAID.PDF
- [4] <http://www.microlab.net>.
- [5] M. Ruan, J. Shen, C.B. Wheeler, *Latching Micromagnetic Relays*, Journal of Microelectromechanical Systems, Vol. 10, No. 4, Dec. 2001.
- [6] F.J. Cadieu, H. Hedge and K. Chen, *The Synthesis of $Sm_2(Co, Fe, Zr)_{17}$ High Energy Product, 16 to 30 MGoe, Thick Sputtered Films*, IEEE Transactions on Magnetics, Vol. 25, no. 5, September 1989.
- [7] H. Hedge, S. U. Chen, and F. J. Cadieu, *Film Sm-Co permanent magnets for the biasing of thin permalloy strips*, Journal of Applied Physics 73 (1993), p.5926.
- [8] Ya.L. Linetsky and N.V. Kornilov, *Structure and Magnetic Properties of Sputtered Nd-Fe-B Alloys*, Journal of Materials Engineering and Performance, Vol. 4(2), April 1995.
- [9] M. Nakano, S. Tsunami, and H. Fukunaga, *Magnetic Properties of Nd-Fe-B Thick Film Magnets Prepared by Laser Ablation Technique*,
- [10] C. Liu and Y.W. Li, *Micromachined Magnetic Actuators Using Electroplated Permalloy*, IEEE Transactions on Magnetics, Vol. 35, no. 3, May 1999.
- [11] W.P. Taylor, O. Brand, M.G. Allen, *Fully Integrated Magnetically Actuated Micromachined Relays*, Journal of Microelectromechanical Systems, Vol. 7, no. 2, June 1998.

- [12] L.K. Lagorce and M.G. Allen, *Micromachined Polymer Magnets*, Proceedings of the Ninth Annual International Workshop on MEMS, MEMS '96, 1996, p.85-90.
- [13] L.K. Lagorce and M.G. Allen, *Magnetic Microactuators Based on Polymer Magnets*, IEEE Journal of Microelectromechanical Systems, vol. 8, no. 1, March 1999.
- [14] H.J. Cho and C.H. Ahn, *A Bidirectionnal Magnetic Microactuator Using Electroplated Permanent Magnet Arrays*, Journal of Microelectromechanical Systems, Vol. 11, no. 1, February 2002.
- [15] T.J. garino, T. Christenson, and E. Venturini, *Fabrication of MEMS devices by powder-filling into DXRL-formed molds*, Materials Science of Microelectromechanical Systems (MEMS) Devices, Boston, MA, USA, pp. 195-200 (1-2 Dec. 1998).
- [16] N.V. Myung, D.Y. Park, M. Schwartz, K. Nobe, H. Yang, C.-K. Yang and J.W. Judy, *Electrodeposited Hard Magnetic Thin Films For MEMS Applications*, Sixth International Symposium on Magnetic Materials, Processes and Devices, Proc. Electrochem. Soc., 2000.
- [17] J. W. Judy and N. Myung, *Magnetic Materials for MEMS*, MRS Workshop on MEMS Materials, San Francisco, California, (April 5-6, 2002), pp. 23-26.
- [18] T.-S. Chin, *Permanent magnet films for applications in microelectromechanical systems*, Journal of Magnetism and Magnetic Materials 209 (2000) 75-79.
- [19] K. Fischer, B. Chaudhuri, S. McNamara, H. Guckel, Y. Gianchandani and D. Novotny, *A Latching, Bistable Optical Fiber Switch Combining Liga Technology with Micromachined Permanent Magnets*, Tech. Dig., IEEE Intl Conf. on Solid-State Sensors and Actuators (Transducers'01), Munich, Germany, June 2001, pp. 1340-1343.
- [20] O. Cugat et al, *Deformable Magnetic Mirror For Adaptive Optics: First Resuts*, 13th annual international conference on Micro Electro Mechanical Systems, 2000. (MEMS 2000).
- [21] P.-A. Gilles, J. Delamare, O. Cugat, J.-L. Schanen, *Design of a permanent magnet planar synchronous micromotor* Conference Record of the 2000 IEEE Industry Applications Conference, Vol. 1, 2000, p. 223-227.
- [22] O. Cugat, *Matériaux magnétiques pour les microsystèmes*, chapter in Cahier de Synthèse du CNRS: Matériaux Magnétiques - décembre 1996.
- [23] Iulica Zana and Giovanni Zangarini, *Co-Pt micromagnets by electrodeposition*, Journal of Applied Physics, vol. 91, 10.
- [24] <http://www.physics.qc.edu/cadieu.htm> Web Page of Professor F.J. Cadieu.

- [25] <http://www.ir.misis.ru>
- [26] <http://www.comadur.ch>
- [27] <http://www.sdmagnetics.com>
- [28] <http://www.us-incorp.com>
- [29] <http://mstd.nrl.navy.mil/Facilities/facilities.html>
- [30] D. Hyman and M. Mehregany, *Contact Physics of Gold Microcontacts for MEMS Switches*, IEEE Transactions on Components and Packaging technologies, vol. 22, no.3, Sept. 1999, p. 357-364.
- [31] B.P. Gogoi and C.H. Mastrangelo, *Adhesion Release and Yield Enhancement of Microstructures Using Pulsed Lorentz Forces*, Journal of Microelectromechanical Systems, vol. 4, no. 4, december 1995.
- [32] F.D. Bannon, J.R. Clark and C.T.-C. Nguyen, *High-Q HF Microelectromechanical Filters*, IEEE Journal of Solid-State Circuits, vol.35, no.4, april 2000.
- [33] C. Bozler, R. Drangmeister, S. Duffy, M. Gouker, J. Knecht, L. Kushner, R. Parr, S. Rabe, L. Travis, *MEMS microswitch arrays for reconfigurable distributed microwave components*, Microwave Symposium Digest., 2000 IEEE MTT-S International, vol. 1, 2000, p. 153 -156.
- [34] D.S. Greywall, *Micromechanical RF Filters excited by the Lorentz Force*, J. Micromech. Microeng., vol.9, p.78-84, 1999.
- [35] R.A. Mc Currie, *Ferromagnetic Materials, Structure and Properties*, Academic Press, 1994.
- [36] V. Milanovic, M. Maharbiz, A. Singh, B. Warneke, Z. Ningning, H.K. Chan, K.S.J. Pister, *Microrelays for batch transfer integration in RF systems*, Micro Electro Mechanical Systems, 2000. MEMS 2000, Jan 2000, p. 787 -792.
- [37] J-W. Park, J.Y. Park, Y-H Joung and M.G. Allen, *Fabrication of High Current and Low Profile Micromachined Inductor With Laminated Ni/Fe Core*, IEEE Transactions on Components and Packaging Technologies, vol.25, no.1, March 2002.
- [38] J.-M. Huang, K.M. Liew, C.H. Wong, S. Rajendran, M.J. Tan, A.Q. Liu, *Mechanical design and optimization of capacitive micromachined switch*, Sensors and Actuators A, no. 93, 2001, p. 273-285.
- [39] M. Géradin, D. Rixen, *Mechanical Vibrations: Theory and Application to Structural Dynamics*, 2nd edition, Wiley, NY, 1997.

- [40] K.J. Binns, P.J. Lawrenson, C.W. Trowbridge, *The Analytical and Numerical Solution of Electric and Magnetic Fields*, Wiley.
- [41] Y. Leroy, M. Guiton and N. Triantafyllidis, *Bifurcation and Stability of an Elastic Plate Over an Inviscid and Buoyant Fluid*, 2001.
- [42] S.H. Gould, *Variational Methods for Eigenvalue Problems*, University of Toronto Press, 1957.